

SWAN: PREPROCESSING SGD ENABLES ADAM-LEVEL PERFORMANCE ON LLM TRAINING WITH SIGNIFICANT MEMORY REDUCTION

Chao Ma*
Microsoft Research

Wenbo Gong*
Microsoft Research

Meyer Scetbon*
Microsoft Research

Edward Meeds
Microsoft Research

* These authors contributed equally to this work.

ABSTRACT

Adaptive optimizers such as Adam (Kingma & Ba, 2015) have been central to the success of large language models. However, they maintain additional moving average states throughout training, which results in memory requirements several times greater than the model. This overhead imposes constraints on scalability and computational efficiency. On the other hand, while stochastic gradient descent (SGD) is optimal in terms of memory efficiency, their capability in LLM training is limited (Zhao et al., 2024b).

To address this dilemma, we show that pre-processing SGD is sufficient to reach Adam-level performance on LLMs. Specifically, we propose to preprocess the instantaneous stochastic gradients with two simple operators: GradNorm and GradWhitening. GradNorm stabilizes gradient distributions, and GradWhitening counteracts the local curvature of the loss landscape, respectively. This results in SWAN (SGD with Whitening And Normalization), a stochastic optimizer that eliminates the need to store any accumulative state variables. Empirically, SWAN has the same memory footprint as SGD, achieving $\approx 50\%$ reduction on total end-to-end memory compared to Adam. In language modeling tasks, SWAN demonstrates the same or even a substantial improvement over Adam. Specifically, when pre-training the LLaMa model with 350M and 1.3B parameters, SWAN achieves a $2\times$ speedup by reaching the same evaluation perplexity in less than half tokens seen.

1 INTRODUCTION

Adaptive optimizers, such as Adam and its variants (Kingma & Ba, 2015; Loshchilov & Hutter, 2019; Shazeer & Stern, 2018; Pagliardini et al., 2024; Liu et al., 2023; Zhao et al., 2024a), have been central to the success of training large language models (LLMs) (Brown et al., 2020; Touvron et al., 2023; Dubey et al., 2024; Bi et al., 2024; Bai et al., 2023; Zhang et al., 2022). However, most adaptive optimizers for LLMs are *stateful*, meaning they require tracking and maintaining internal states. While achieving remarkable empirical success, these states introduce significant memory overhead. For instance, Adam (Kingma & Ba, 2015)—the de facto optimizer for LLM training—involves the tracking of exponential moving averages (EMAs), effectively doubling memory requirements. AdEMAMix (Pagliardini et al., 2024) – an extension of Adam that achieves significant convergence speed boost – requires storing even more states, tripling the memory requirements. This overhead can be significant especially in distributed settings, where the optimizer states could consume a significant amount of the GPU memory (Dubey et al., 2024; Korthikanti et al., 2023). On the other hand, while stochastic gradient descent (SGD) is optimal in terms of memory efficiency (i.e., they are *stateless*), their capability to train LLMs is limited (Zhao et al., 2024b), and the performance gap between SGD and Adam is significant (Zhang et al., 2020; Kunstner et al., 2023; 2024).

To address the memory-performance dilemma for LLMs, this work questions the requirement of accumulative state variables during training to achieve good performance in LLMs. We propose

to simply preprocess the instantaneous SGD gradient in a history-independent manner, such that it still preserves certain desirable properties of adaptive optimizers. This result in SWAN (SGD with Whitening And Normalization), a novel SGD-like optimizer that eliminates *all* internal optimizer states and empirically surpasses the performance Adam on several LLM pre-training scenarios.

Our proposed optimizer consists of two stateless operators applied to the raw gradients: GradNorm and GradWhitening. GradNorm aims to *stabilize* the stochasticity of gradient distributions during training, while GradWhitening seeks to *neutralize* the local geometry of the loss landscape. Both operators enables SWAN to rely solely on the statistics of the current gradient matrices. This SGD preprocessing approach eliminates all internal optimizer states, and therefore reproduces the memory consumption of SGD, reaching a new state-of-the-art in terms of optimizer memory efficiency for LLMs ($\approx 50\%$ reduction on end-to-end memory footprint vs Adam, and $\approx 100\%$ reduction in optimizer states. See Figure 1). In addition to memory savings, SWAN also demonstrates significant computational efficiency: our empirical evaluations on pre-training LLaMA models on the C4 dataset with multiple model sizes show consistently better performance than Adam and other low-rank memory-efficient optimizers. Remarkably, at the 350M and 1.3B scale, our method achieves 2X faster convergence in terms of tokens seen compared to Adam, marking SWAN the first known stateless optimizer converges as fast/faster than Adam in training large language models.

Our contributions are as follows:

- **A practical, stateless, adaptive optimizer.** SWAN (Algorithm 1), is a novel optimizer based on preprocessing SGD with two stateless operators —GradNorm and GradWhitening (Figure 2). They perform gradient stabilization and loss landscape whitening, respectively, using information solely from the current gradient. SWAN offers the following properties crucial in practice:
 1. Robustness to ill-conditioned problems. On LLM pretraining, SWAN converges quickly even *without learning rate warm-ups* (Section 5, Section 5.6), a property not observed in Adam.
 2. Memory efficiency: SWAN achieves the memory footprint of SGD, that is $\approx 50\%$ reduction on total memory, and $\approx 100\%$ reduction on optimizer states when compared to Adam.
 3. Computational efficiency: consistently outperforms Adam and reaches up to $2\times$ acceleration and effective throughput.
- **Theoretical analysis of SWAN.** We show that (1) GradNorm can be derived as a strategy to stabilize the heterogeneous covariance of LLM gradients, leveraging the redundancies in LLM gradient flows (Theorem 1 in Appendix B); and (2) GradWhitening can be derived as a non-diagonal second-order update under a specific structural assumption of the Hessian (Section 4.3). Additionally, we highlight that GradWhitening leads to convergence rates that are robust to the condition number of the local curvature (Theorem 3, Appendix B.3), offering theoretical advantages over SGD and Adam (Proposition 3).
- **Fast convergence for LLM pretraining tasks.** Through experiments (Section 5) on LLM pretraining tasks, we demonstrate that SWAN not only reduces memory overhead but also outperforms Adam and other memory-efficient optimizers. Notably, SWAN achieves convergence speed-ups of over $2\times$ in terms of the number of tokens used for both 350M and 1.3B models (Figure 1).

2 PRELIMINARIES

One of the most used adaptive optimizers is the Adam optimizer (Kingma & Ba, 2015). Adam is an example of *stateful* optimizers, which involves tracking and maintaining internal states. It combines the advantages of two earlier methods: AdaGrad (Duchi et al., 2011), which adapts learning rates based on the historical gradient magnitude, and RMSProp (Tieleman, 2012), which mitigates the aggressive decrease in learning rates by using a decaying average of squared gradients.

Consider a loss function $\mathcal{L}_{\mathbf{W}} : \mathcal{X} \rightarrow \mathbb{R}$, parameterized by weight matrices $\mathbf{W} \in \mathbb{R}^{m \times n}$, and denote $\mathbf{x}^{(t)}$ a mini-batch of inputs provided at the t -th training step that is sampled from data distribution $p_{\text{data}}(\mathbf{x})$. Let $\mathbf{G}^{(t)}$ be the stochastic gradient of $\mathcal{L}_{\mathbf{W}}$ (i.e., a random variable induced by sampling

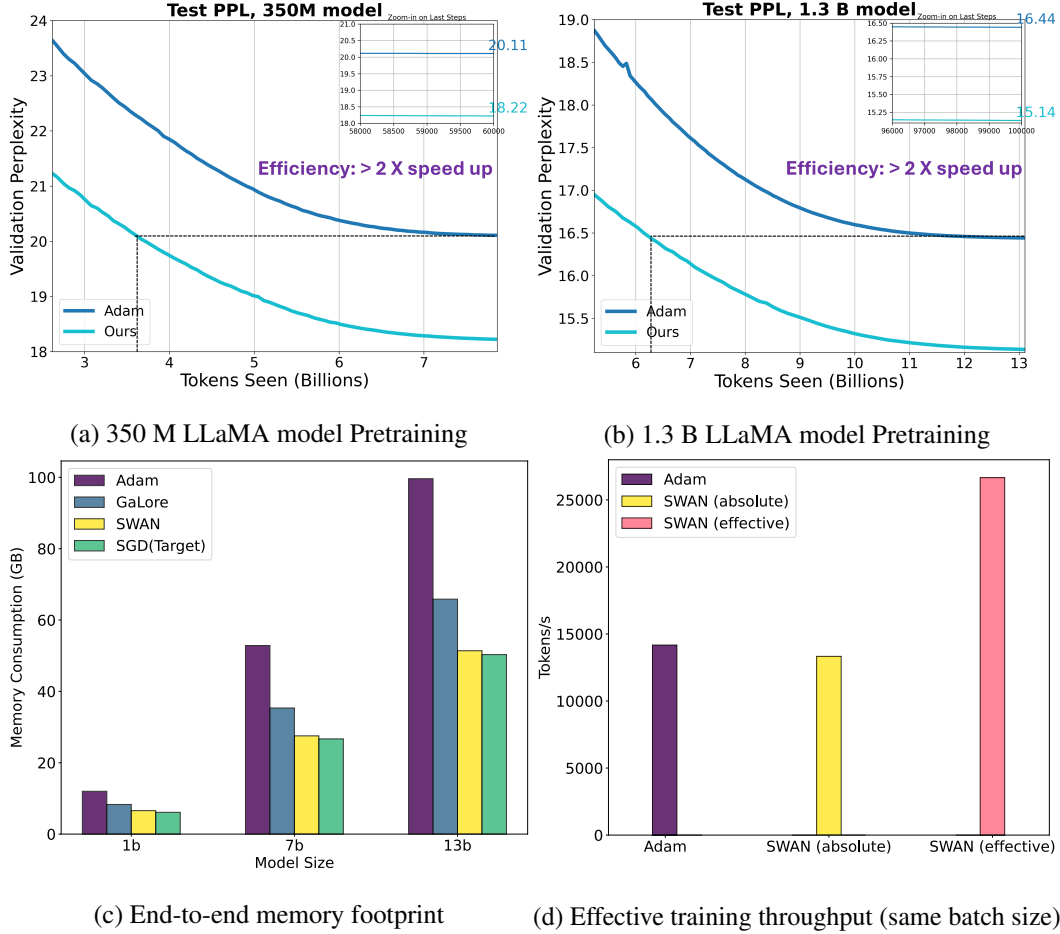


Figure 1: **SWAN performance preview on LLM pretraining.** (a) and (b): On both 350M and 1.3B Llama architectures, SWAN achieves > 2X speed-up vs Adam in terms of tokens seen. (c): memory footprint. Unlike Zhao et al. (2024a), we directly measure end-to-end memory under full-model training, with batch size = 1 sequence. SWAN achieves near-SGD optimizer memory reduction ($\approx 50\%$ reduction on total memory, and $\approx 100\%$ reduction on optimizer states). (d) Training throughput analysis on training 1.3 B model on $4 \times A100$, under constant batch size = 130K tokens. We present two metrics: absolute throughput, measured by number of training tokens consumed per second; and effective throughput, which is absolute throughput adjusted by the efficiency of optimizer relative to Adam. SWAN closely reproduces the absolute throughput of Adam, while improving the effective throughput.

$\mathbf{x}^{(t)}$). Then, Adam can be broken down into the following steps:

$$\begin{aligned}
 \mathbf{G}^{(t)} &= \nabla_{\mathbf{W}} \mathcal{L}_{\mathbf{W}}(\mathbf{x}^{(t)}), & \mathbf{x}^{(t)} &\sim p_{\text{data}}(\mathbf{x}) && \text{(stochastic gradient)} \\
 \mathbf{m}^{(t)} &= \beta_1 \mathbf{m}^{(t-1)} + (1 - \beta_1) \mathbf{G}^{(t)}, &&&& \text{(EMA first moment)} \\
 \boldsymbol{\nu}^{(t)} &= \beta_2 \boldsymbol{\nu}^{(t-1)} + (1 - \beta_2) \mathbf{G}^{(t)2}, &&&& \text{(EMA second moment)} \\
 \mathbf{W}^{(t+1)} &= \mathbf{W}^{(t)} - \eta \left(\frac{\hat{\mathbf{m}}^{(t)}}{\sqrt{\hat{\boldsymbol{\nu}}^{(t)} + \epsilon}} \right) &&&& \text{(weight update)}
 \end{aligned}$$

where $\mathbf{m}^{(t)}$ and $\boldsymbol{\nu}^{(t)}$ are EMAs of the first and second moments of the gradients; and η is a global step size. Essentially, Adam estimates the signal-to-noise (SNR) ratios and use it to adjust learning rates element-wise. Tracking and storing these two EMA estimates triple the total memory consumption required to train a LLM model. For example, for LLaMA 405B model, storing model weights requires 810 GB of memory, while the Adam optimizer states requires an additional 1.6TB of memory.

Desired properties of Adam. There is a rich literature on understanding adaptive methods’ inner workings and unreasonable effectiveness. Notably, the key desired properties of Adam can be categorized as *gradient smoothing*, *gradient invariance* and *gradient whitening*. (1) *Gradient smoothing*: the EMA operations in Adam naturally reduce the influence of mini-batch noise [Cutkosky & Mehta \(2020\)](#); [Crawshaw et al. \(2022\)](#); (2) *Gradient invariance*: recent work suggest the performance gap between SGD and Adam might lie in Adam’s *sign-descent*-like nature ([Bernstein et al., 2018](#); [Crawshaw et al., 2022](#); [Chen et al., 2023](#)). For example, Adam is robust to the rescaling of gradient diagonals ([Kingma & Ba, 2015](#)); and is invariant to any sign-preserving scalings (under $\beta_1 = \beta_2 = 0$)([Bernstein et al., 2018](#)). And (3) *Gradient whitening* : it is well-known that the second moment EMA of Adam approximates the diagonal of Fisher information matrix ([Kingma & Ba, 2015](#); [Hwang, 2024](#)), and biases the optimization trajectories towards well-conditioned regions ([Jiang et al., 2024](#)). For a more comprehensive discussion of these properties, please refer to appendix A.

Adam as SGD preprocessing, and the potential unnecessary of EMAs Adam can be viewed as history-dependent preprocessing of the gradients ($\{\mathbf{G}^{(0)}, \mathbf{G}^{(1)}, \dots, \mathbf{G}^{(t-1)}, \mathbf{G}^{(t)}\} \rightarrow \frac{\hat{m}^{(t)}}{\sqrt{\hat{v}^{(t)} + \epsilon}}$) to achieve the desired properties above. A key observation is, all of the above properties are achieved through the element-wise operations. That is, each element of the gradient matrix is pre-processed and re-scaled independently. This ignores the interactions and structures among different variables, and we hypothesize this is the reason why extra history information is need to compensate this gap, leading to the requirement of EMA states. Thus, we believe that designing stateless adaptive optimizers is possible, if we can achieve similar properties by designing new matrix-level operations that are preprocesses the instantaneous gradients of SGD ($\mathbf{G}^{(t)} \rightarrow \hat{\mathbf{G}}^{(t)}$).

3 THE SWAN OPTIMIZER: PREPROCESSING SGD WITH NORMALIZATION AND WHITENING

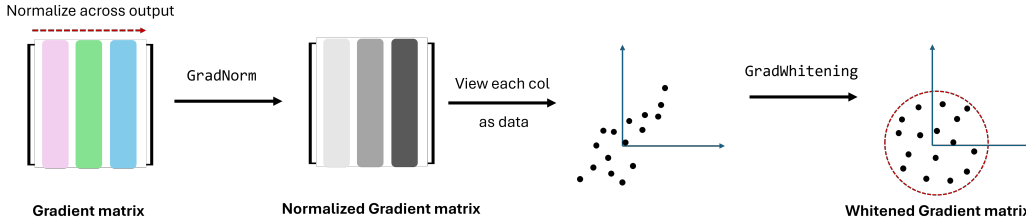


Figure 2: Illustration of GradNorm and GradWhitening operators. In GradNorm operator, we perform standardization across the output dimensions (columns), using statistics computed row-wise. In GradWhitening operator, we treat each column (or row) of the gradient matrix \mathbf{G} as a separate data sample. Then, the GradWhitening operator can be seen as stretching/squeezing the gradient data along all eigen directions, such that the covariance matrix is an identity matrix. Note that the same approach can be applied row-wise as well.

As discussed in Section 2, we believe the key to designing stateless, adaptive, and effective optimizers lies in designing new *matrix-level* operations that exploit rich information in the gradient matrix. To this end, we propose a new stateless optimizer (Algorithm 1), SWAN (SGD with Whitening And Normalization). SWAN preprocesses SGD based on two simple operators, GradNorm and GradWhitening, both are *stateless, matrix-level* operators. When applied in tandem, they achieve similar desirable properties of adaptive optimizers, without the need to store historical gradient moments. In this section we describe the update rules of SWAN.

3.1 SWAN UPDATE RULES

In SWAN (Algorithm 1), the raw SGD gradient \mathbf{G}^t is processed by the following operations ¹:

¹Here \mathbf{G} is assumed to be the gradient matrix for some parameter block in the model (e.g. a linear layer); enabling us to take advantage of the matrix structure to achieve our smoothing and whitening goals.

Algorithm 1 SWAN Optimizer

Input: weight matrix $\mathbf{W} \in \mathbb{R}^{m \times n}$ with $m \leq n$. Step size η . Number of GradWhitening iteration k .
Initialize step $t \leftarrow 0$
repeat
 $\mathbf{G}^{(t)} \in \mathbb{R}^{m \times n} \leftarrow \nabla_{\mathbf{W}^{(t)}} \mathcal{L}^{(t)}(\mathbf{W}^{(t)})$
 $\tilde{\mathbf{G}}^{(t)} \leftarrow \text{GradNorm}(\mathbf{G}^{(t)})$
 $\Delta \mathbf{W}^{(t)} \leftarrow \text{GradWhitening}(\tilde{\mathbf{G}}^{(t)}, k)$
(optional) $\Delta \mathbf{W}^{(t)} \leftarrow \frac{\|\tilde{\mathbf{G}}^{(t)}\| \Delta \mathbf{W}^{(t)}}{\|\Delta \mathbf{W}^{(t)}\|}$
 $\mathbf{W}^{(t)} \leftarrow \mathbf{W}^{(t-1)} - \eta \Delta \mathbf{W}^{(t-1)}$
 $t \leftarrow t + 1$
until convergence criteria met
return $\mathbf{W}^{(t)}$

Algorithm 2 GradWhitening Operator

Input: Matrix $\mathbf{G}^{m \times n}$ with $m \leq n$. Number of Newton Schultz iteration k , step size β
Initialize $\mathbf{Y} \leftarrow \mathbf{G}\mathbf{G}^\top$, $\mathbf{Z} \leftarrow \mathbf{I}$
for $i = 1, \dots, k$ **do**
 $\mathbf{Y} \leftarrow \beta \mathbf{Y} (3\mathbf{I} - \mathbf{Z}\mathbf{Y})$,
 $\mathbf{Z} \leftarrow \beta (3\mathbf{I} - \mathbf{Z}\mathbf{Y})\mathbf{Z}$
end for
return $\mathbf{Z}\mathbf{G}$

Algorithm 3 GradNorm Operator

Input: Matrix $\mathbf{G}^{m \times n}$
return $\frac{\mathbf{G} - \frac{1}{n} \sum_{j=1}^n \mathbf{G}_{:,j} \mathbf{1}_n^\top}{\sqrt{\frac{1}{n} \sum_{j=1}^n (\mathbf{G}_{:,j} - \sum_{j=1}^n \mathbf{G}_{:,j})^2 \mathbf{1}_n^\top}}$

Figure 3: SWAN Optimizer. Note that for GradWhitening, in principle, any approximate algorithms can be applied, such as matrix Pade approximant. Here we only show one particular working example based on Newton-Schulz, which introduces minimal overheads.

$$\begin{cases} \tilde{\mathbf{G}}^{(t)} \leftarrow \text{GradNorm}(\mathbf{G}^{(t)}) \\ \Delta \mathbf{W}^{(t)} \leftarrow \text{GradWhitening}(\tilde{\mathbf{G}}^{(t)}) \end{cases} \quad (\text{SWAN})$$

The weight is then updated by $\mathbf{W}^{(t+1)} = \mathbf{W}^{(t)} - \eta \Delta \mathbf{W}^{(t)}$. The GradNorm operator (Equation (1)) normalizes the gradient matrix row-wise (Figure 2); and the GradWhitening operator whitens (Figure 2) the gradients. These operators are described as below.

GradNorm: gradient invariance & stabilization. Consider the gradient matrix $\mathbf{G} \in \mathbb{R}^{m \times n}$ with rows and columns corresponding to input and output dimensions, respectively, of some block of model parameters. Let $1 \leq i \leq m$ represent the input indices and $1 \leq j \leq n$ represent the output indices. Instead of performing element-wise EMA to stabilize and normalize the noisy gradients, we propose to standardization across the output dimensions at each time step t , defined as:

$$\text{GradNorm}(\mathbf{G}) = \frac{\mathbf{G} - \bar{\mathbf{g}} \mathbf{1}_n^\top}{s \mathbf{1}_n^\top} \quad (1)$$

where $\bar{\mathbf{g}} = \frac{1}{n} \sum_{j=1}^n \mathbf{G}_{:,j}$ is the mean across output dimensions at time t ; $s = \sqrt{\frac{1}{n} \sum_{j=1}^n (\mathbf{G}_{:,j} - \bar{\mathbf{g}})^2}$ is the standard deviation across dimensions at time t ; $\bar{\mathbf{g}}$ and s are m -dimensional column vectors; and $\mathbf{1}_n$ is a n -dimensional column vector of ones.

GradNorm is an example of operators typically used in the forward pass applied to the backward pass: GradNorm is LayerNorm (Ba et al., 2016) (without learnable parameters) being applied to the *backward* gradient rather than *forward* activations. Similar to Layer Norm, GradNorm allows the optimizer to be invariant under the following transformations on gradient matrix: i) matrix-wise re-scaling; ii) matrix-wise re-centering; iii) row-wise re-scaling; and iv) row-wise re-centering. Compared to the sign operation ($\text{sign}(\mathbf{G})$) and matrix-wise normalization ($\frac{\mathbf{G}}{\|\mathbf{G}\|}$) used in signed descent, GradNorm preserves richer information of the gradient scaling while offering invariance properties. Moreover, in Section 4 we will show that when applied to a transformer architecture, GradNorm also helps stabilize the gradient distribution across time.

GradWhitening: gradient whitening. Adam performs approximate gradient whitening *element-wise*, leading to well-conditioned regions. In contrast, we propose the matrix GradWhitening operator, which performs whitening at the *matrix level*. Given the gradient \mathbf{G} , the GradWhitening

operator simply orthogonalizes \mathbf{G} ²:

$$\text{GradWhitening}(\mathbf{G}) := (\mathbf{G}\mathbf{G}^\top)^{-\frac{1}{2}}\mathbf{G} \quad (2)$$

where the exponent $-\frac{1}{2}$ stands for matrix inverse square root. One can show that $(\mathbf{G}\mathbf{G}^\top)^{-\frac{1}{2}}\mathbf{G}$ is simply the orthogonalization of \mathbf{G} , i.e., the closest orthogonal matrix to \mathbf{G} (w.r.t the Frobenius norm).

Along with GradNorm, GradWhitening is an example of applying forward pass operators to the backward pass: GradWhitening is decorrelated batch normalization (Huang et al., 2018; Li et al., 2018) applied to the *backward* gradient rather than *forward* activations. As shown in Figure 2, if we treat each column of \mathbf{G} as i.i.d. vector-valued data samples $\mathbf{G} = \{\mathbf{g}_1, \dots, \mathbf{g}_j, \dots, \mathbf{g}_n\}$, GradWhitening can be seen as effectively stretching/squeezing this data matrix along the eigenvectors while whitening its covariance to be identity (hence the name *whitening*). This essentially forces the gradients to *traverse all eigen-directions at the same rate*, and is therefore more robust to local geometries of the optimization problem. In Section 4, we will show that GradWhitening makes implicit structural assumptions of Hessian/Fisher information matrix that emerge from transformers.

3.2 PRACTICAL CONSIDERATIONS

Various GPU-friendly and fast approximations are developed in the literature of decorrelated batch normalization or feature whitening. We consider the *naive* Newton-Schulz (N-S) iteration algorithm (Li et al., 2018; Huang et al., 2019) to compute GradWhitening:

$$\mathbf{Y}_{k+1} = \frac{1}{2}\mathbf{Y}_k(3\mathbf{I} - \mathbf{Z}_k\mathbf{Y}_k), \quad \mathbf{Z}_{k+1} = \frac{1}{2}(3\mathbf{I} - \mathbf{Z}_k\mathbf{Y}_k)\mathbf{Z}_k \quad (3)$$

where $\mathbf{Y}_0 = \mathbf{G}\mathbf{G}^\top$ ³, $\mathbf{Z}_0 = \mathbf{I}$. At convergence, $\text{GradWhitening}(\mathbf{G}) = \mathbf{Z}\mathbf{G}$ (Algorithm 2).

Computational Overhead. In practice, we only run the Newton-Schulz for 5-10 iterations, which corresponds to 25-50 matrix multiplications. However, we found this has negligible computational overhead (< 5%) w.r.t the 2x speed-up in LLM pre-training obtained (see Section 5). These matrix multiplications are highly parallelizable so that in practice, for the task of training LLMs, the batch-size is the more dominant factor for compute. For example QWen 14B (Bai et al., 2023) has 4M batch size vs a model dimension $d_{\text{model}} = 5120$, DeepSeek (Bi et al., 2024) 67B has 6M batch size vs $d_{\text{model}} = 8192$, and LLama 3 (Dubey et al., 2024) 405B has 4-16M batch size vs $d_{\text{model}} = 16384$. To estimate the computational overhead, we derive the following ratio. Assuming the N-S iteration involves approximately $25 \times d_{\text{model}}^3$ FLOPs. In contrast, the primary training cost scales with the batch size and is proportional to $\text{batch_size} \times d_{\text{model}}^2$ FLOPs. In those examples, the estimated computational overhead of Newton-Schulz is typically below $\leq 5\%$. This ensures the additional computational cost remains minimal compared to the overall training cost. This is validated in our throughput benchmarking in Section 5.5.

Rescaling GradWhitening. The whitening operation GradWhitening maps the normalized gradient $\tilde{\mathbf{G}}^{(t)}$ onto the closest orthogonal matrix, hence might drastically change the effective learning rate. In practice, we propose the following re-scaling before updating the weight:

$$\Delta\mathbf{W}^{(t)} \leftarrow \frac{\|\tilde{\mathbf{G}}^{(t)}\|\Delta\mathbf{W}^{(t)}}{\|\Delta\mathbf{W}^{(t)}\|} \quad (4)$$

This will help us to rescale the norm of whitened gradient back to the norm of $\tilde{\mathbf{G}}^{(t)}$, and allowing us to get reasonably good performance without extensively tuning learning rates—we found that the learning rates used Adam usually also work well for SWAN. It is also possible to remove rescaling, but that would require additional hyper-parameter search to find the optimal learning-rate for SWAN.

²An equivalent definition is given by $\text{GradWhitening}(\mathbf{G}) = \mathbf{U}\mathbf{V}^\top$, where \mathbf{U} and \mathbf{V} are both orthogonal matrices defined via SVD decomposition of $\mathbf{G} = \mathbf{U}\mathbf{S}\mathbf{V}^\top$.

³It is standard practice (Li et al., 2018; Huang et al., 2019) to normalize the singular values of \mathbf{G} before Newton-Schulz iteration, i.e., $\mathbf{G} \leftarrow \mathbf{G}/\|\mathbf{G}\|$.

4 ANALYSIS: A LLM LEARNING DYNAMICS PERSPECTIVE

As a new stateless adaptive optimizer, the complete theoretical properties of SWAN is an open question which we leave for future work. However, as a first analysis, we consider SWAN from a *learning dynamics* perspective, specifically the dynamics of an LLM based upon a simplified transformer block. It is this analysis that led to the design of SWAN.

4.1 SETUP

We assume the following simplified transformer block (STB) architecture recently proposed in [Tian et al. \(2023\)](#):

Definition 1 (Simplified Transformer Block (STB)). *Given the input activation $\mathbf{x} \in \mathbb{R}^{M_C \times 1}$, query token index q , context embedding matrix $\mathbf{U}_C \in \mathbb{R}^{d \times M_C}$, and the query embedding $\mathbf{u}_q \in \mathbb{R}^{d \times 1}$, the STB computes the output $\mathbf{h} \in \mathbb{R}^{n \times 1}$ as $\mathbf{h} = \phi(\mathbf{W}^\top (\mathbf{U}_C (\exp(\mathbf{z}_q) \odot \mathbf{x}) + \mathbf{u}_q))$, where M_C is the context length, the attention logits $\mathbf{z}_q \in \mathbb{R}^{M_C \times 1}$ are given by $z_{ql} = \mathbf{u}_q^\top \mathbf{W}_Q^\top \mathbf{W}_K \mathbf{u}_l$, with $\mathbf{W}_Q, \mathbf{W}_K \in \mathbb{R}^{d \times d}$ being weight matrices for the queries and keys, respectively, $\mathbf{W} \in \mathbb{R}^{d \times n}$ is the weight matrix for the feedforward network, and ϕ is a nonlinearity function such as the ReLU.*

Given a STB, we consider a loss function $\mathcal{L}_{\mathbf{W}, \mathbf{z}}(\mathbf{x}^{(t)})$, where $\mathbf{x}^{(t)}$ is a mini-batch of inputs provided at the t -th training step sampled from data distribution $p_{\text{data}}(\mathbf{x})$. Standard mini-batch learning dynamics is then given by

$$\dot{\mathbf{W}}^{(t)} = \frac{\partial \mathcal{L}_{\mathbf{W}, \mathbf{z}_q}(\mathbf{x}^{(t)})}{\partial \mathbf{W}}, \quad \dot{\mathbf{z}}_q^{(t)} = \frac{\partial \mathcal{L}_{\mathbf{W}, \mathbf{z}_q}(\mathbf{x}^{(t)})}{\partial \mathbf{z}_q}.$$

In this case, both $\dot{\mathbf{W}}^{(t)}$ and $\dot{\mathbf{z}}_q$ are viewed as random variables induced by random mini-batch $\mathbf{x}^{(t)}$. For example, for each row i , $\dot{\mathbf{W}}^{(t)}[i, :]$ can be re-written as $\dot{\mathbf{W}}^{(t)}[i, :] = \mathbb{E}[\dot{\mathbf{W}}^{(t)}[i, :]] + \varepsilon_{\mathbf{W}}^{(t)}[i, :]$, where $\varepsilon_{\mathbf{W}}^{(t)}[i, :]$ is zero mean random variable with covariance $\text{Cov}[\dot{\mathbf{W}}^{(t)}[i, :]]$.

4.2 GradNorm STABILIZES GRADIENT DISTRIBUTIONS OF SIMPLIFIED TRANSFORMERS

As discussed in Section 3, GradNorm contains rich information of the gradient scaling while offering invariance properties over certain transformations. Here we show that, based on the dynamics of the STB, GradNorm also stabilizes $\varepsilon_{\mathbf{W}}^{(t)}$:

Theorem 1 (GradNorm stabilizes gradient distributions across time for the STB). *Consider the STB (Definition 1). Assuming we inherit the assumptions in Theorem 1 of [Tian et al. \(2023\)](#), as described in Appendix B. Then consider $\mathbf{U}_C^\top \mathbf{W}$, the composition of the MLP project-up matrix and the embedding matrix as a whole. Then, its standardized stochastic gradients $\tilde{\mathbf{G}}_{\mathbf{U}_C^\top \mathbf{W}}^{(t)} := \text{GradNorm}(\frac{\partial \mathcal{L}_{\mathbf{W}, \mathbf{z}}(\mathbf{x}^{(t)})}{\partial \mathbf{U}_C^\top \mathbf{W}})$ satisfy:*

$$\text{Cov}[\tilde{\mathbf{G}}_{\mathbf{U}_C^\top \mathbf{W}}^{(t_1)}[i, :]] = \text{Cov}[\tilde{\mathbf{G}}_{\mathbf{U}_C^\top \mathbf{W}}^{(t_2)}[i, :]] \quad \text{for all } t_1, t_2, \text{ and } i.$$

In other words, the covariance structure of $\tilde{\mathbf{G}}$ is identical across all time steps t , achieving distributional stability across time. The same relationship also holds for the gradient of attention score $\tilde{\mathbf{G}}_{\mathbf{z}_q}^{(t)} := \text{GradNorm}(\frac{\partial \mathcal{L}_{\mathbf{W}, \mathbf{z}_q}(\mathbf{x}^{(t)})}{\partial \mathbf{z}_q})$.

Theorem 1 suggests that GradNorm implicitly aligns with the dynamics of transformer architectures and removes the time-heterogeneity in gradient covariance structures.

4.3 GradWhitening IS AN EFFICIENT NON-DIAGONAL SECOND-ORDER UPDATE

In this section, we show that GradWhitening is equivalent to non-diagonal approximate second-order method, under a specific Kronecker factorization assumption of the Hessian. The assumption is as below:

Assumption 1 (Assumption of GradWhitening). *At time t , the local Hessian \mathbf{H} of the loss has shared block-diagonal structure, such that $\mathbf{H} = \mathbf{I}_{n \times n} \otimes \tilde{\mathbf{H}}$, where $\tilde{\mathbf{H}} \in \mathbb{R}^{m \times m}$.*

By leveraging this structural assumption, we can now effectively estimate \mathbf{H} by only using one single gradient matrix sample $\mathbf{G} := [\mathbf{g}_1, \dots, \mathbf{g}_n] \in \mathbb{R}^{m \times n}$. Recall that the Fisher information formulation of Hessian is defined as $\mathbf{H} = \mathbb{E}(\text{Vect}(\mathbf{G})\text{Vect}(\mathbf{G})^\top)$ where $\text{Vect}(\cdot)$ denotes the vectorized operation. Under assumption 1, we can estimate $\mathbf{H} = \mathbf{I}_{n \times n} \otimes \tilde{\mathbf{H}}$, using a single sample of the gradient, that is we can compute the following simple estimate $\frac{1}{n} \sum_{i=1}^n \mathbf{g}_i \mathbf{g}_i^\top = \mathbf{G} \mathbf{G}^\top$, which approximate the current $\tilde{\mathbf{H}}$. Hence, GradWhitening can be seen as applying a second order update under our structural assumption:

$$\text{GradWhitening}(\mathbf{G}) = (\mathbf{G} \mathbf{G}^\top)^{-\frac{1}{2}} \mathbf{G} = \tilde{\mathbf{H}}^{-\frac{1}{2}} \mathbf{G}$$

In Theorem 2 of Appendix, we will further show that the pre-conditioned update rule $\tilde{\mathbf{H}}^{-\frac{1}{2}} \mathbf{G}$ indeed induces a Newton-like behavior. More importantly, in the following Proposition, we show that the implicit assumption of GradWhitening is a good abstraction of LLM dynamics since it in fact aligns with the equilibrium Hessian structure in the STB regime:

Proposition 1 (Shared structures in the block-diagonal of Hessians at transformer equilibrium). *Consider a STB (1), trained with full-batch gradient descent. Next, assume we inherit all the assumptions from Theorem 1 of Tian et al. (2023). Then, as $t \rightarrow \infty$, we have the following shared Hessian structure along the diagonal blocks:*

$$\frac{\mathbf{H}_{sk,s'k}}{\sum_{s,s'} \mathbf{H}_{sk,s'k}} \rightarrow \frac{\mathbf{H}_{sk',s'k'}}{\sum_{s,s'} \mathbf{H}_{sk',s'k'}}, \quad \forall 1 \leq s, s' \leq d, 1 \leq k, k' \leq n \quad (5)$$

Where $\mathbf{H}(\mathbf{W})_{sk,s'k'} = \frac{\partial^2 \mathcal{L}}{\partial w_{sk} \partial w_{s'k'}}$.

Proposition 1 shows that, under a simplified setting of the transformer, the Hessian will also converge to an equilibrium solution where the $M_C \times M_C$ blocks over the diagonal direction of Hessian shares the identical structure, which supports the implicit assumption of GradWhitening. This result is verified in our numerical experiment (Appendix, Figure 9).

Finally, Theorem 3 presented in Appendix will also how GradWhitening helps to make the convergence rate of SGD more robust to the condition number of local curvatures, and outperforms both SGD and Adam in the ill-conditioned regime.

5 EXPERIMENTS

In this section, we perform empirical studies on SWAN. The main goals of those studies are as follows:

- Verifying whether GradNorm and GradWhitening indeed effectively fulfilled their design goals (stabilizing gradient noise, and modeling/counteracting local curvatures). This is performed in Section 5 and Section 5.
- Verifying whether SWAN can consistently offer Adam-level or even better performance, while maintaining low memory cost and high-throughput. This is performed in Section 5, Section 5 and Section 5.5, respectively.
- Ablation study (Section 5.6).

All experiments run on NVIDIA A100 GPUs.

5.1 DOES GRADNORM STABILIZE GRADIENT DISTRIBUTIONS OF SGD?

To investigate whether GradNorm indeed stabilizes stochastic gradient distributions as claimed in Theorem 1, we conduct a series of controlled experiments using a scaled-down version of the LLaMA architecture. We aim to assess the impact of GradNorm on the gradient distribution during training by analyzing the statistical properties of gradients across multiple training steps. Specifically, we employ a small-scale LLaMA-based model with approximately 10 million parameters (Lialin et al., 2023). Training is conducted on the C4 dataset (Raffel et al., 2020).

Baselines We compare the following methods:

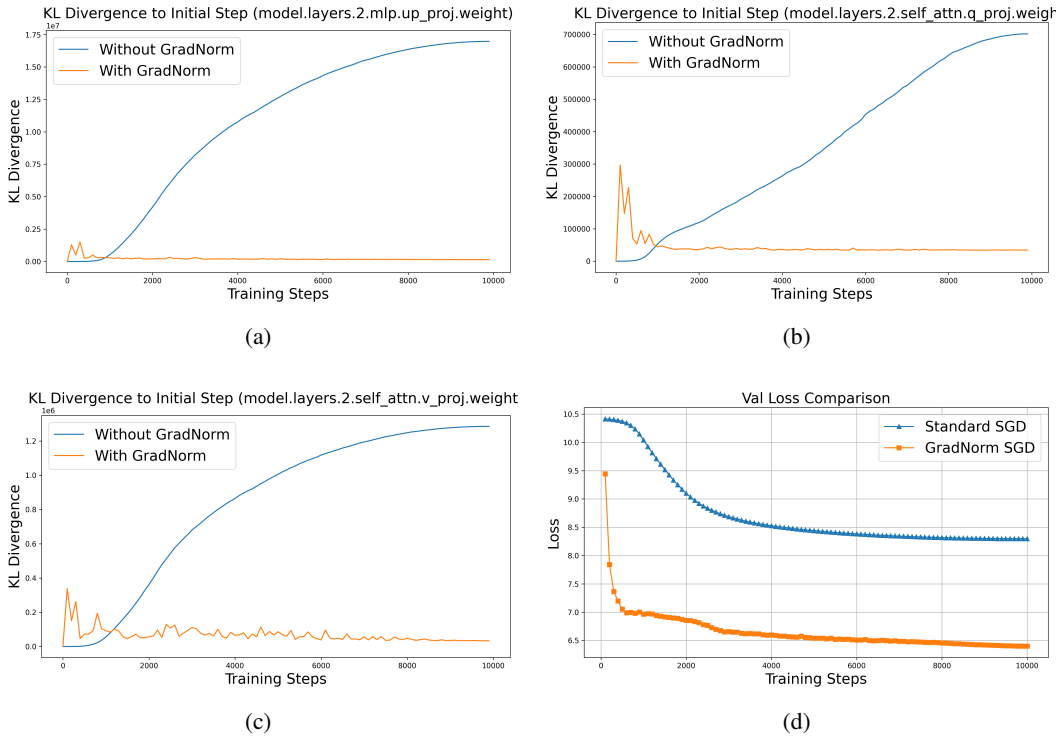


Figure 4: (a) - (c): KL Divergence of gradient distributions across training Steps. We use the projection weights in attention and MLP modules of the second layer as an example. The plots compare standard training with GradNorm-augmented training. Lower KL divergence values indicate greater stability in gradient distributions. (d): Training loss curve comparing standard training vs GradNorm-augmented training

- Standard training: this baseline utilize SGD optimizer with a learning rate of $5 \times e^{-4}$, and apply a linear learning rate scheduler with a warm-up period comprising 10% of the total training steps (10,000).]
- GradNorm-augmented training: apply GradNorm on noisy gradients before SGD update. We use the same hyperparameters as the SGD baseline.

Methodology For each method, we measure the change of gradient statistics due to mini-batch sampling noise. For each training step, after the parameter update, we additionally sample 16 different mini-batches (each with batch size 64), and calculate the mean and standard deviation of the corresponding gradients on each of those batches. Then, we estimate the Kullback-Leibler divergence between the current gradient distribution (raw gradient and with GradNorm) relative to the initial distribution at $t = 0$. This allows us to quantify the temporal evolution of gradient distributions.

Results Figure 4 illustrates the KL divergence of gradient distributions over training steps for both standard training and GradNorm-augmented training, relative to the initial distribution at $t = 0$. Apart from minor spikes in the beginning of training, GradNorm consistently and effectively stabilizes the gradient noise distribution. Furthermore, as a by-product, the loss curves demonstrate that models trained with GradNorm performs indeed improves upon standard training.

Ablation One question that we might ask is this: is the performance boost of GradNorm simply due to that fact that GradNorm might be increasing the effective learning rate. We conduct detailed ablation experiments in Section 5.6, in a larger scale setting, which show this is not the case. These findings validate the hypothesis that GradNorm serves as an effective mechanism for mitigating the adverse effects of mini-batch noise on gradient distributions, thereby enhancing the stability and performance of the training process.

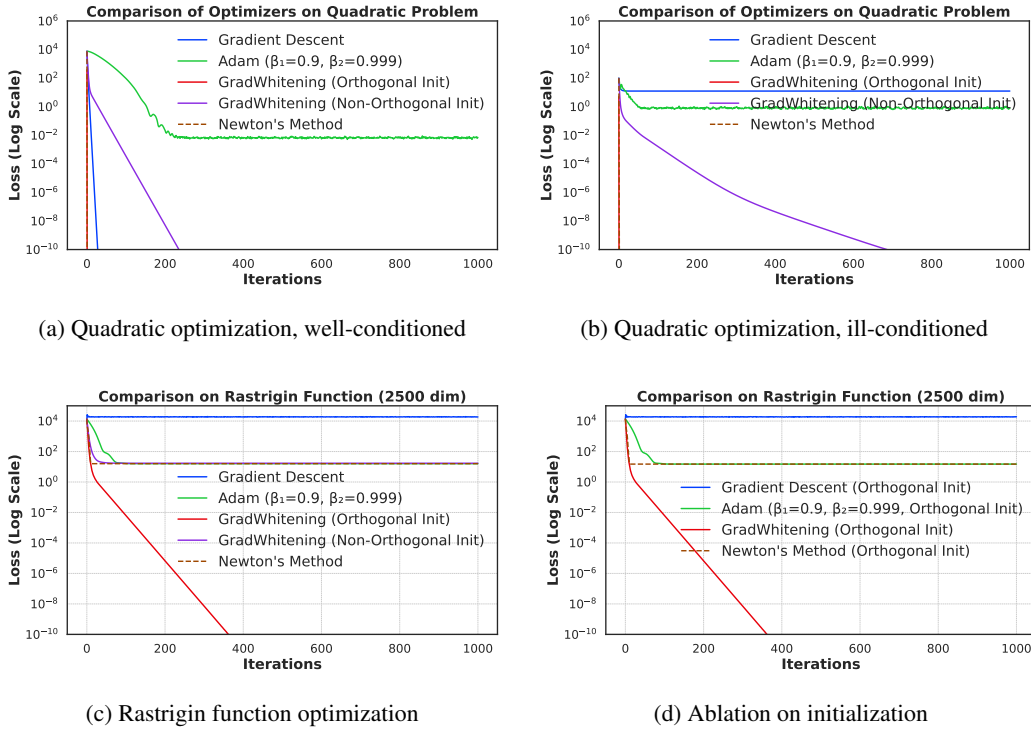


Figure 5: Comparison of convergence rate of different methods on quadratic and non-convex optimization problems. (a): 2500-dimensional quadratic optimization with well-conditioned \mathbf{H} . (b): 2500-dimensional quadratic optimization with ill-conditioned \mathbf{H} (c): 2500-dimensional Rastrigin function optimization. (d): 2500-dimensional Rastrigin function optimization, but forcing all methods to use the same orthogonal initial location.

5.2 DOES GradWhitening COUNTERACTS LOCAL CURVATURE AND PROVIDE FAST CONVERGENCE ON ILL-CONDITIONED PROBLEMS?

We aim to evaluate the pure optimization capability of GradWhitening processed gradient descent on classic optimization problems. We consider the following three settings:

- **High-dimensional quadratic optimization.** We construct quadratic optimization problem of the form in Equation (23), with $\mathbf{W} \in \mathbb{R}^{50 \times 50}$.
- **Ill-conditioned quadratic optimization.** We construct a quadratic optimization problem with the same dimensionality and formulation as above, but this time we deliberately choose an ill-conditioned \mathbf{H} .
- **Non-convex optimization with multiple local optimas.** We consider the following multi-variate Rastrigin function:

$$f(\mathbf{W}) = m^2 \mathbf{A} + \frac{1}{2} \text{Tr}[\mathbf{W}^\top \mathbf{W}] - \mathbf{A} \sum_{ij} \cos(2\pi W_{ij})$$

where \mathbf{W} is $m \times m$ matrix. This function has 10^{m^2} possible local optima. This is a complicated stress test for optimization algorithms, where many methods are expected to fail at different regimes. We set $m = 50$, and compare the same methods as in the previous experiment.

Baselines On all three settings (quadratic, quadratic ill-conditioned, and Rastrigin) we compare 5 different methods, including 3 baselines and 2 GradWhitening based variants. For baselines, we have: gradient descent (with theoretical optimal learning rate in Theorem 4); Adam ($\beta_1 = 0.9, \beta_2 = 0.999$ with hand-tuned learning rate); and Newton's method with tuned learning rate. For 2

Table 1: Comparison with Adam and its memory-efficient low-rank variants on pre-training various sizes of LLaMA models on C4 dataset. Validation perplexity is reported, along with a memory estimate of the total of parameters and optimizer states based on BF16 format. Since we used train scripts and configs based on the code openourced by Zhao et al. (2024a), all baseline results are taken from Zhao et al. (2024a). The exceptions are the results for Adam and Galore, as we cannot exactly reproduce the results reported in Zhao et al. (2024a); hence we reported results from our own runs instead.

	60M	130M	350M	1.3 B
SWAN	32.28 (0.12G)	24.13 (0.25G)	18.22 (0.68G)	15.13 (2.60G)
Adam	33.02 (0.36G)	24.44 (0.76G)	20.11 (2.06G)	16.44 (7.80G)
Galore	33.09 (0.24G)	24.67 (0.52G)	19.74 (1.22G)	15.89 (4.38G)
Low-Rank	78.18 (0.26G)	45.51 (0.54G)	37.41 (1.08G)	142.53 (3.57G)
LoRA	34.99 (0.36G)	33.92 (0.80G)	25.58 (1.76G)	19.21 (6.17G)
ReLoRA	37.04 (0.36G)	29.37 (0.80G)	29.08 (1.76G)	18.33 (6.17G)
SWAN speed up vs Adam	1.2 X	1.23 X	> 2X	> 2X
r of low-rank methods	128	256	256	512
Training Tokens	1.1B	2.2B	6.4B	13.1B

GradWhitening-based methods, we consider: GradWhitening-augmented GD with orthogonal initialization (i.e., $\mathbf{W}^{(0)\top} \mathbf{W}^{(0)} = \mathbf{I}$); and without orthogonal initialization. This is to verify whether the claims of Theorem 2 and Theorem 3 is true (i.e., GradWhitening-processed GD behaves like Newton’s method under orthogonal initialization). All methods are initialized with the same initial condition (apart from GradWhitening with orthogonal initialization, which will project the original initialization onto the orthogonal version).

Results Results are shown in Figure 5, (a) - (c). Main findings are summarized as follows:

- On quadratic optimization problems (Figure 5 (a) and (b)), GradWhitening with orthogonal initialization and Newton’s method converges to optimal solution with 1 step of optimization, confirming our theoretical prediction in Theorem 2 and Theorem 3.
- On quadratic optimization problems (Figure 5 (a)), when the problem is well-conditioned, standard GD outperforms both Adam and GradWhitening (non-orthogonal initialization). However, when the problem becomes ill conditioned (Figure 5 (b)), GradWhitening (non-orthogonal initialization) outperforms GD by a large margin; while GD suffers from convergence.
- In all three settings (Figure 5, (a) - (c)), GradWhitening with non-orthogonal initialization consistently outperforms Adam, confirming our theoretical results in Proposition 3.
- On Rastrigin function optimization (Figure 5 (c)), GradWhitening performs competitively to Newton’s method, with or without orthogonal initialization.

Ablation Furthermore, we additionally conduct ablation study on the effect of initialization locations, as shown in fig. 5 (d). In this case, we force all methods to use the same orthogonalized initialization location for optimization. As shown by the result, GradWhitening still consistently outperforms all baselines, eliminating the potential hypothesis that orthogonalized initialization gave GradWhitening an unfair advantage.

5.3 SWAN PERFORMANCE ON LLM PRE-TRAINING TASKS

Setup Finally, we present results on the task of pre-training large language models. Below we consider LLaMa architecture used in Zhao et al. (2024a) with RMSNorm and SwiGLU activations. We consider sizes of 60M, 130M, 350M and 1.3B parameters on C4 dataset Raffel et al. (2020), trained with an effective batch size of 130K tokens (512 batchsize and 256 context length). SWAN is applied to all linear modules (in both attention and MLP layers). We run all experiments with BF16 format by default.

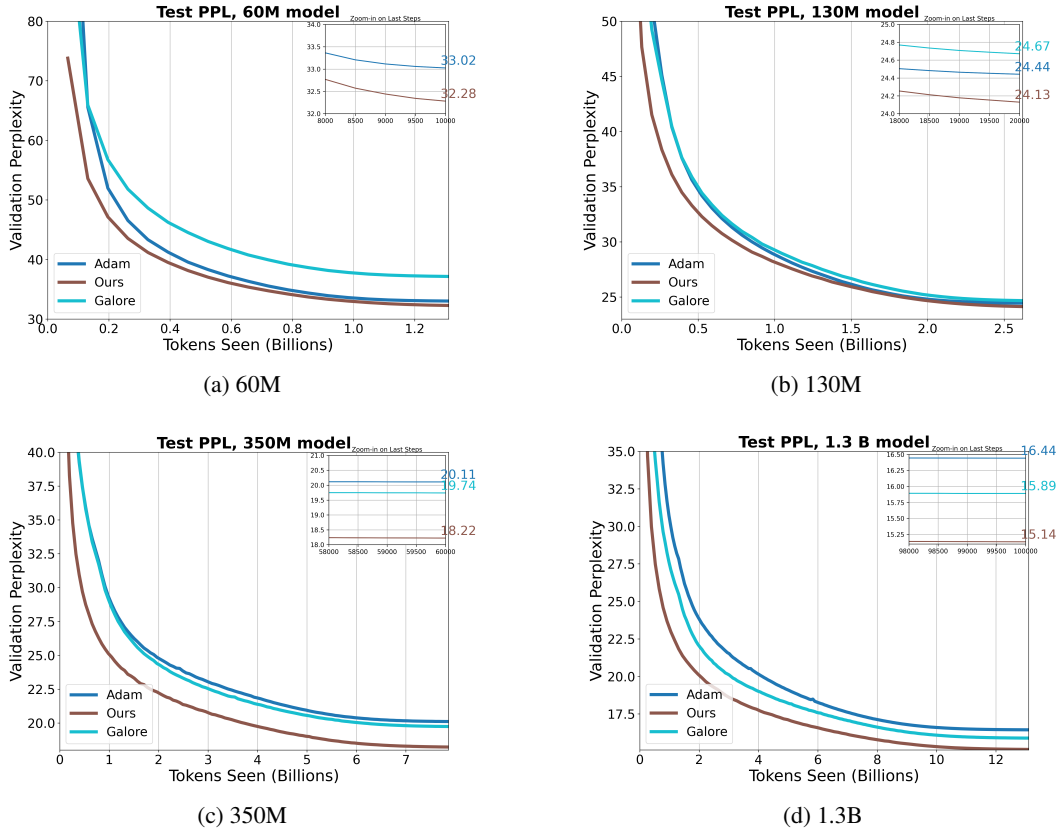


Figure 6: Comparison of convergence rate of different methods on LLM pretraining tasks.

Baselines Since the main goal of SWAN is to explore the feasibility of EMA-free adaptive optimizers for LLMs, we mainly compare to Adam and its memory efficient variants. We use the exact evaluation settings of Zhao et al. (2024a); along with Adam, these include:

- **Galore** Zhao et al. (2024a): the state-of-the-art memory efficient variant of Adam that based on low-rank projections of gradients.
- **Low-Rank** (Kamalakara et al., 2022): Low-rank reparameterization of the weights with the trainable factorization $W = BA$.
- **LoRA**: LoRA Hu et al. (2021) applied for pre-training in the exact setting as used in Zhao et al. (2024a).
- **ReLoRA** Lialin et al. (2023): a full-rank learning extension of Lora with parameter merging.

Hyperparameters For all baselines, we directly apply the same hyperparameter configs (including model configs, optimizers, schedulers) open sourced by Zhao et al. (2024a)⁴. This includes method-specific fine-tuned optimal learning rates obtained via searching on fixed grid Zhao et al. (2024a). For our SWAN method, we simply use a hand-picked default hyperparameter setting out-of-the-box, without fine tuning. These include a un-tuned, default learning rate of 0.001 across all models, and the 10 steps of Newton-Schultz iteration. Notably, thanks to the strong robustness offered by GradWhitening to ill-conditioned problems, SWAN can safely start training *without* any learning rate warm-up. This is not the case for other baselines such as Adam, in which they failed to converge without long warm-ups in our ablation experiments. Apart from the warm-up hyperparameter, all the rest of the parameters in learning rate scheduling used by SWAN is the same as all other baselines.

⁴This does not include Adam, since the authors of Zhao et al. (2024a) did not disclose their Adam configs. However, we used the same learning rate sweep procedure as described in their paper. This result in an optimal learning rate of 0.001 for 60M, 130M and 350M models, and 0.0007 for 1.3 B models. These are also consistent with the optimal learning rates found in some other works, such as Pagliardini et al. (2024).

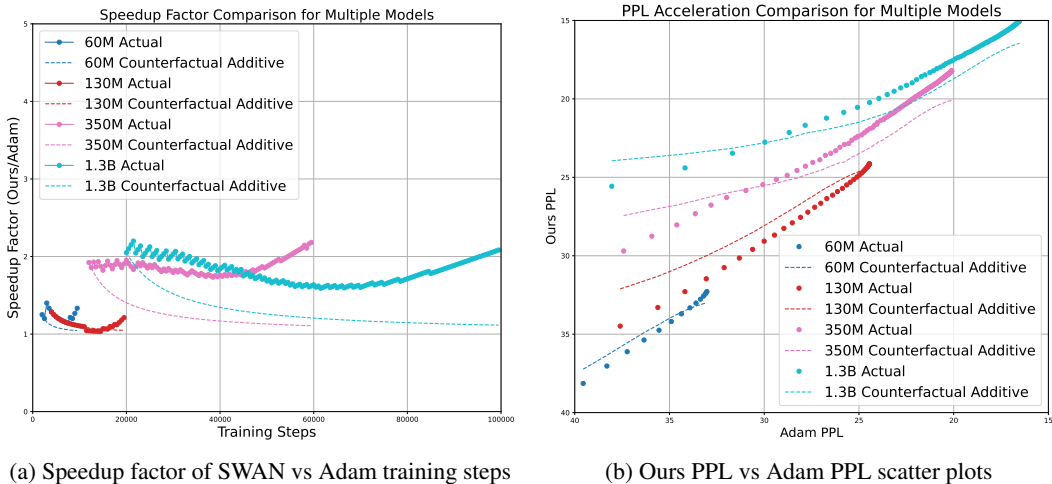


Figure 7: Comparative analysis of SWAN and Adam optimizers: speedup ratios and perplexity metrics across various model sizes. **(a)** shows how SWAN reduces the number of training steps needed to achieve the same evaluation perplexity as Adam for models ranging from 60M to 1.3B parameters. A speedup ratio greater than one indicates that SWAN reaches target PPL values faster than Adam. **(b)** presents a direct comparison of perplexity scores between SWAN and Adam. In both plots, we also provide counterfactual additive curves (dashed lines) modeling baselines corresponding to constant step advantages. Together, these plots highlight the nature of SWAN’s speedup over Adam across different model scales.

Remark on fair comparison As empirically shown in [Kaddour et al. \(2024\)](#), it is essential to use the same training budget when comparing efficient optimizers; unfortunately, this fact was not widely respected in some recent work of efficient algorithms. [Kaddour et al. \(2024\)](#) showed that certain state-of-the-art efficient optimizers has shown no gain over Adam under the same training budget. Therefore, in our experiments above, we exactly follow the rule of equal training budget (in our case, defined in terms number of tokens), and forces all methods to have learning rate fully decayed to the same target learning rate at the end of optimization. For a even fairer comparison, we left the learning rates of SWAN untuned.

Results Results are shown in [Table 1](#) and [Figure 6](#). SWAN outperforms all baselines in both validation PPLs, as well as estimated memory consumption (SWAN theoretically should consume the same memory as SGD). Furthermore, to our surprise, on both 350M and 1.3B models, SWAN achieved > 2X speed up against Adam in terms of number of steps (hence number of tokens), see [Figure 1](#) and [Figure 7 \(a\)](#). More in-depth discussion of speed-up will be provided in [Section 5](#).

5.4 IS THE IMPROVEMENT MULTIPLICATIVE OR ADDITIVE?

One natural question when evaluating speedup factors is whether our method provides a *multiplicative* or *additive* speedup over Adam. Specifically, multiplicative speedup indicates an optimizer’s performance advantage over a baseline increases proportionally with time, maintaining a consistent speed-up ratio. This is the ideal scenario we would like to achieve. In contrast, additive speed-up implies only a fixed, constant advantage in steps over baseline, which is less desired. To investigate this, we utilize two plots: the *speed-up ratio comparison* and the *perplexity comparison* ([Figure 7](#)), across different model sizes. Before understanding those plots, we first introduce the following concepts:

Speedup ratio definition The *speedup ratio* $R(P)$ is defined as the ratio of the number of training steps Adam requires to reach a specific evaluation perplexity (PPL) to the number of steps SWAN requires to achieve the same PPL. Mathematically, for a given PPL threshold P , the speedup ratio is expressed as:

$$R(P) = \frac{S_{\text{Adam}}(P)}{S_{\text{SWAN}}(P)} \tag{6}$$

where $S_{\text{Adam}}(P)$ and $S_{\text{SWAN}}(P)$ denote the training steps taken by Adam and SWAN, respectively, to reach perplexity P .

Counterfactual additive curve estimation To determine if the speed-up is additive, we estimate a *counterfactual additive curve* by assuming a constant step advantage Δ of SWAN over Adam. This is calculated using the first 10% - 20% (depending on the number of maximum steps) of the training data:

$$\Delta = \frac{1}{N} \sum_{i=1}^N (S_{\text{Adam}}(P_i) - S_{\text{SWAN}}(P_i)) \quad (7)$$

where N is the number of PPL thresholds within the initial 10% - 20% of training steps.

For the speedup ratio plot:

$$R_{\text{additive}}(P) = \frac{S_{\text{Adam}}(P)}{S_{\text{Adam}}(P) - \Delta} \quad (8)$$

For the perplexity comparison plot:

$$\text{PPL}_{\text{additive}}(S) = \text{PPL}_{\text{Adam}}(S + \Delta) \quad (9)$$

This represents the expected perplexity of SWAN if it only consistently outperforms Adam by Δ steps.

Results Results are shown in Figure 7. In both subplots, the *actual* performance of SWAN is compared against the *counterfactual additive curves*. If the actual plot lies significantly above the counterfactual additive curve, it indicates a stronger tendency towards multiplicative speedup, meaning SWAN’s performance gains are more than just a fixed step advantage. Analyzing models of sizes 60M, 130M, 350M, and 1.3B parameters, we observe that:

- For smaller models (60M and 130M parameters), the actual speedup ratios closely follow the counterfactual additive curves, suggesting that the speedup of SWAN over Adam is primarily additive.
- For larger models (350M and 1.3B parameters), the actual plots significantly exceed the counterfactual additive curves, and has a clear sign of accelerated growth. This pronounced deviation indicates a multiplicative speedup, demonstrating that SWAN offers increasingly substantial efficiency gains as model complexity scales.

5.5 MEMORY EFFICIENCY AND THROUGHPUT ANALYSIS

This section, we benchmark the memory footprint of SWAN as well as its throughput.

Memory footprint We benchmark the memory footprint of SWAN, Adam, and Galore in a practical scenario.. Unlike Zhao et al. (2024a) where memory is benchmarked under a layer-wise training strategy, we directly measure end-to-end memory under full-model training, with batch size = 1 sequence, across different model sizes (1.3B, 7B, and 13B). Results are shown in Figure 1 (c), SWAN achieves near-theoretical limit of optimizer memory efficiency of full-parameter training (assuming no quantization). This means that SWAN can reproduce the memory footprint of vanilla SGD, reaching $\approx 50\%$ reduction on total memory, and $\approx 100\%$ reduction on optimizer states. This result again highlights the advantage of the stateless design.

Effective throughput To measure the throughput of SWAN, we consider training a 1.3 B model on $4 \times \text{A100}$, under constant batch size = 130K tokens. Here We present two metrics: absolute throughput, measured by number of training tokens consumed per second; and effective throughput, which is absolute throughput adjusted by the efficiency of optimizer relative to Adam. The purpose of the first metric (absolute throughput) is to measure whether SWAN (especially the use of N-S iterations in GradWhitening) create a significant drop in training throughput; and the second metric (effective throughput) takes into account the fact that different optimizers utilizes training tokens at different efficiency level. Results are shown in Figure 1 (d), SWAN closely reproduces the absolute throughput of Adam, implying that unlike full SVD used in (Zhao et al., 2024a), the computational

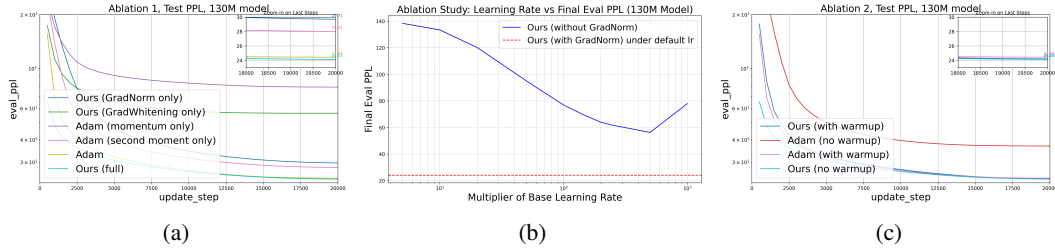


Figure 8: Ablation studies on 130M model. (a) Ablation on the contribution of each components in SWAN and Adam. (b) Ablation on removing GradNorm and compensate with larger learning rates. (c) Ablation on the effect of learning rate warm-ups.

overhead of GradWhitening is minimal. As a result, SWAN has doubled the effective throughput vs Adam, due to its high token utilization efficiency as shown in Section 5. All results are obtained using GradWhitening in BF16 format.

5.6 ABLATION STUDIES

How does GradNorm and GradWhitening contribute to the performance boost? We consider the following 6 ablation settings: SWAN(full), SWAN (GradNorm only), SWAN (GradWhitening only), Adam (full), Adam (momentum only), and Adam (second moment only). Results are shown in Figure 8 (a). It suggests that both GradNorm and GradWhitening makes significant contribution towards the final performance of SWAN; and removing any of them results in suboptimal performance. This is similar to how the first and second moment EMAs of Adam jointly contributes to the final performance.

Is it true that SWAN works only because its GradNorm component might have increased the effective learning rates? To answer this question, we remove the GradNorm component of SWAN, and perform learning rate sweep for it. We start from the default base learning rate used by full SWAN, and then scale it with multipliers ranging from 1 to 10^3 . Results are shown in Figure 8 (b), where the final validation ppl of SWAN without GradNorm under different learning rate multipliers are shown in blue line; and the performance of the full SWAN under default learning rate is shown as a dashed red reference line. The result suggests that, although increasing the effective learning rates might improve the performance of SWAN without GradNorm, there is still a significant gap between SWAN without GradNorm and the full SWAN. Together with results in Section 5, we can conclude that the gradient noise stabilization of GradNorm is indeed essential, and it cannot be trivialized as larger effective learning rates.

How does warm-up affect the performance? In Section 5, we showed that SWAN does not need any learning rate warm-ups and can train with large learning rates (the default 0.001 learning rate used by all methods is considerably large in LLMs settings). Here we perform ablation and compare Adam and SWAN both under warm-ups and not warm-ups. As suggested by the results in Figure 8 (c), we found that for SWAN, training without learning rate warm-ups indeed gives better performance. Meanwhile, SWAN still outperforms Adam (with warm-up) under the same warm-up schedule of Adam. On the contrary, Adam only works with proper learning rate warmup. If we remove warmups, the performance of Adam becomes drastically worse. This confirms our claim that SWAN is more robust to the local geometries of the optimization problems and can work without (and with) learning rate warm ups.

6 RELATED WORKS

Low-rank memory efficient methods Low-rank memory-efficient optimizers have become pivotal in training large language models (LLMs) by reducing memory consumption while maintaining model performance. A foundational approach in this domain is LORA introduced by Hu et al. (2021), which fine-tunes pre-trained models using low-rank adaptors for each layer, thereby minimizing the memory footprint. This leads a full line of low-rank adaptation research, but they are mostly focused

on post-training adaptations. More recently, ReLoRA [Lialin et al. \(2023\)](#), FLORA [Hao et al. \(2024\)](#) and Galore [Zhao et al. \(2024a\)](#) further push the boundaries of memory-efficient pre-training for LLMs, by introducing the idea of using low-rank projection of gradients to achieve full-rank learning. They have demonstrated significant memory savings on optimizer states, with relatively low impact on model performance. However, these methods often require 30–50 % of the full Adam’s states and may underperform in terms of convergence speed and final model quality ([Zhao et al., 2024a](#)). Moreover, it is still an open question on the design choices of these methods, for example: how and why to choose low-rank subspace and projectors? Are these projections properly used, given the non-exchangeability nature between low-rank projection and Adam EMA operator? Why spikes in loss curves are observed during subspace are shifted/mixed ([Chen et al., 2024](#))? These unaddressed questions might make the behavior of low-rank gradient optimizers unpredictable in practice.

Non-adaptive methods with partial EMA removal. Lion ([Chen et al., 2023](#)) and Signum ([Bernstein et al., 2018](#)) have introduced effective ways to simplify optimization by partially removing the exponential moving average (EMA) of the second moment. These methods reduce memory and computational overhead while retaining the benefits of momentum through the first moment EMA, offering a practical trade-off between simplicity and performance. However, their reliance on momentum inherently limits their extension to further remove both first and second moment EMAs are removed, as both would reduce to SignSGD ([Bernstein et al., 2018](#)), which lacks the adaptive learning rate capability of Adam. This might explain why sign-based methods have limited success in LLM pre-training tasks ([Chen et al., 2023](#); [Liu et al., 2023](#)). On the contrary, our approach completely removes all EMA terms while maintaining the adaptive learning rate nature, which is the key to the success of modern adaptive optimizers.

7 CONCLUSION

The most important insight that we conclude for the paper is, preprocessing SGD might already be enough for LLM training tasks. This presents an elegant solution to address the memory-performance dilemma of training LLMs using adaptive optimizers like Adam. The other insight comes from the fact that the key components of the SWAN optimizer were designed using key insights from LLM dynamics under a simplified setting. In that sense, this paper serves as a proof-of-concept on the value of studying the dynamics of LLM architectures when designing optimizers. We hope both research insights can inspire more research along this line to further advance this field.

REFERENCES

- Jimmy Ba, Jamie Ryan Kiros, and Geoffrey E. Hinton. Layer normalization. *ArXiv*, abs/1607.06450, 2016. URL <https://api.semanticscholar.org/CorpusID:8236317>.
- Jinze Bai, Shuai Bai, Yunfei Chu, Zeyu Cui, Kai Dang, Xiaodong Deng, Yang Fan, Wenbin Ge, Yu Han, Fei Huang, et al. Qwen technical report. *arXiv preprint arXiv:2309.16609*, 2023.
- Jeremy Bernstein, Yu-Xiang Wang, Kamyar Azizzadenesheli, and Animashree Anandkumar. signsgd: Compressed optimisation for non-convex problems. In *International Conference on Machine Learning*, pp. 560–569. PMLR, 2018.
- DeepSeek-AI Xiao Bi, Deli Chen, Guanting Chen, Shanhuang Chen, Damai Dai, Chengqi Deng, Honghui Ding, Kai Dong, Qiusi Du, Zhe Fu, Huazuo Gao, Kaige Gao, Wenjun Gao, Ruiqi Ge, Kang Guan, Daya Guo, Jianzhong Guo, Guangbo Hao, Zhewen Hao, Ying He, Wen-Hui Hu, Panpan Huang, Erhang Li, Guowei Li, Jiashi Li, Yao Li, Y. K. Li, Wenfeng Liang, Fangyun Lin, Aixin Liu, Bo Liu (Benjamin Liu), Wen Liu, Xiaodong Liu, Xin Liu, Yiyuan Liu, Haoyu Lu, Shanghao Lu, Fuli Luo, Shirong Ma, Xiaotao Nie, Tian Pei, Yishi Piao, Junjie Qiu, Hui Qu, Tongzheng Ren, Zehui Ren, Chong Ruan, Zhangli Sha, Zhihong Shao, Jun-Mei Song, Xuecheng Su, Jingxiang Sun, Yaofeng Sun, Min Tang, Bing-Li Wang, Peiyi Wang, Shiyu Wang, Yaohui Wang, Yongji Wang, Tong Wu, Yu Wu, Xin Xie, Zhenda Xie, Ziwei Xie, Yi Xiong, Hanwei Xu, Ronald X Xu, Yanhong Xu, Dejian Yang, Yu mei You, Shuiping Yu, Xin yuan Yu, Bo Zhang, Haowei Zhang, Lecong Zhang, Liyue Zhang, Mingchuan Zhang, Minghu Zhang, Wentao Zhang, Yichao Zhang, Chenggang Zhao, Yao Zhao, Shangyan Zhou, Shunfeng Zhou, Qihao Zhu, and Yuheng Zou. Deepseek llm: Scaling open-source language models with longtermism. *ArXiv*, abs/2401.02954, 2024. URL <https://api.semanticscholar.org/CorpusID:266818336>.
- Tom B. Brown, Benjamin Mann, Nick Ryder, Melanie Subbiah, Jared Kaplan, Prafulla Dhariwal, Arvind Neelakantan, Pranav Shyam, Girish Sastry, Amanda Askell, Sandhini Agarwal, Ariel Herbert-Voss, Gretchen Krueger, Tom Henighan, Rewon Child, Aditya Ramesh, Daniel M. Ziegler, Jeffrey Wu, Clemens Winter, Christopher Hesse, Mark Chen, Eric Sigler, Mateusz Litwin, Scott Gray, Benjamin Chess, Jack Clark, Christopher Berner, Sam McCandlish, Alec Radford, Ilya Sutskever, and Dario Amodei. Language models are few-shot learners. In *NeurIPS*, 2020.
- Xi Chen, Kaituo Feng, Changsheng Li, Xunhao Lai, Xiangyu Yue, Ye Yuan, and Guoren Wang. Fira: Can we achieve full-rank training of llms under low-rank constraint? *arXiv preprint arXiv:2410.01623*, 2024.
- Xiangning Chen, Chen Liang, Da Huang, Esteban Real, Kaiyuan Wang, Hieu Pham, Xuanyi Dong, Thang Luong, Cho-Jui Hsieh, Yifeng Lu, and Quoc V. Le. Symbolic discovery of optimization algorithms. In *NeurIPS*, 2023.
- Michael Crawshaw, Mingrui Liu, Francesco Orabona, Wei Zhang, and Zhenxun Zhuang. Robustness to unbounded smoothness of generalized signsgd. *Advances in neural information processing systems*, 35:9955–9968, 2022.
- Ashok Cutkosky and Harsh Mehta. Momentum improves normalized sgd. In *International conference on machine learning*, pp. 2260–2268. PMLR, 2020.
- André Belotto Da Silva and Maxime Gazeau. A general system of differential equations to model first-order adaptive algorithms. *Journal of Machine Learning Research*, 21(129):1–42, 2020.
- Abhimanyu Dubey, Abhinav Jauhri, Abhinav Pandey, Abhishek Kadian, Ahmad Al-Dahle, Aiesha Letman, Akhil Mathur, Alan Schelten, Amy Yang, Angela Fan, Anirudh Goyal, Anthony Hartshorn, Aobo Yang, Archi Mitra, Archie Sravankumar, Artem Korenev, Arthur Hinsvark, Arun Rao, Aston Zhang, Aurélien Rodriguez, Austen Gregerson, Ava Spataru, Baptiste Rozière, Bethany Biron, Binh Tang, Bobbie Chern, Charlotte Caucheteux, Chaya Nayak, Chloe Bi, Chris Marra, Chris McConnell, Christian Keller, Christophe Touret, Chunyang Wu, Corinne Wong, Cristian Canton Ferrer, Cyrus Nikolaidis, Damien Allonsius, Daniel Song, Danielle Pintz, Danny Livshits, David Esioibu, Dhruv Choudhary, Dhruv Mahajan, Diego Garcia-Olano, Diego Perino, Dieuwke Hupkes, Egor Lakomkin, Ehab AlBadawy, Elina Lobanova, Emily Dinan, Eric Michael Smith, Filip Radenovic, Frank Zhang, Gabriel Synnaeve, Gabrielle Lee, Georgia Lewis Anderson, Graeme Nail,

- Grégoire Mialon, Guan Pang, Guillem Cucurell, Hailey Nguyen, Hannah Korevaar, Hu Xu, Hugo Touvron, Iliyan Zarov, Imanol Arrieta Ibarra, Isabel M. Kloumann, Ishan Misra, Ivan Evtimov, Jade Copet, Jaewon Lee, Jan Geffert, Jana Vranes, Jason Park, Jay Mahadeokar, Jeet Shah, Jelmer van der Linde, Jennifer Billock, Jenny Hong, Jenya Lee, Jeremy Fu, Jianfeng Chi, Jianyu Huang, Jiawen Liu, Jie Wang, Jiecao Yu, Joanna Bitton, Joe Spisak, Jongsoo Park, Joseph Rocca, Joshua Johnstun, Joshua Saxe, Junteng Jia, Kalyan Vasuden Alwala, Kartikeya Upasani, Kate Plawiak, Ke Li, Kenneth Heafield, and Kevin Stone. The llama 3 herd of models. *CoRR*, abs/2407.21783, 2024.
- John C. Duchi, Elad Hazan, and Yoram Singer. Adaptive subgradient methods for online learning and stochastic optimization. *J. Mach. Learn. Res.*, 12:2121–2159, 2011. URL <https://api.semanticscholar.org/CorpusID:538820>.
- Yongchang Hao, Yanshuai Cao, and Lili Mou. Flora: Low-rank adapters are secretly gradient compressors. *ArXiv*, abs/2402.03293, 2024. URL <https://api.semanticscholar.org/CorpusID:267412117>.
- Edward J Hu, Yelong Shen, Phillip Wallis, Zeyuan Allen-Zhu, Yuanzhi Li, Shean Wang, Lu Wang, and Weizhu Chen. Lora: Low-rank adaptation of large language models. *arXiv preprint arXiv:2106.09685*, 2021.
- Lei Huang, Dawei Yang, Bo Lang, and Jia Deng. Decorrelated batch normalization. In *Proceedings of the IEEE Conference on Computer Vision and Pattern Recognition*, pp. 791–800, 2018.
- Lei Huang, Yi Zhou, Fan Zhu, Li Liu, and Ling Shao. Iterative normalization: Beyond standardization towards efficient whitening. In *Proceedings of the IEEE/CVF conference on computer vision and pattern recognition*, pp. 4874–4883, 2019.
- Dongseong Hwang. Fadam: Adam is a natural gradient optimizer using diagonal empirical fisher information. *arXiv preprint arXiv:2405.12807*, 2024.
- Stanisław Jastrzębski, Zachary Kenton, Devansh Arpit, Nicolas Ballas, Asja Fischer, Yoshua Bengio, and Amos Storkey. Three factors influencing minima in sgd. *arXiv preprint arXiv:1711.04623*, 2017.
- Kaiqi Jiang, Dhruv Malik, and Yuanzhi Li. How does adaptive optimization impact local neural network geometry? *Advances in Neural Information Processing Systems*, 36, 2024.
- Jean Kaddour, Oscar Key, Piotr Nawrot, Pasquale Minervini, and Matt J Kusner. No train no gain: Revisiting efficient training algorithms for transformer-based language models. *Advances in Neural Information Processing Systems*, 36, 2024.
- Siddhartha Rao Kamalakara, Acyr Locatelli, Bharat Venkitesh, Jimmy Ba, Yarin Gal, and Aidan N Gomez. Exploring low rank training of deep neural networks. *arXiv preprint arXiv:2209.13569*, 2022.
- Diederik P. Kingma and Jimmy Ba. Adam: A method for stochastic optimization. In *ICLR (Poster)*, 2015.
- Vijay Anand Korthikanti, Jared Casper, Sangkug Lym, Lawrence McAfee, Michael Andersch, Mohammad Shoeybi, and Bryan Catanzaro. Reducing activation recomputation in large transformer models. *Proceedings of Machine Learning and Systems*, 5:341–353, 2023.
- Frederik Kunstner, Jacques Chen, Jonathan Wilder Lavington, and Mark Schmidt. Noise is not the main factor behind the gap between sgd and adam on transformers, but sign descent might be. *arXiv preprint arXiv:2304.13960*, 2023.
- Frederik Kunstner, Robin Yadav, Alan Milligan, Mark Schmidt, and Alberto Bietti. Heavy-tailed class imbalance and why adam outperforms gradient descent on language models. *arXiv preprint arXiv:2402.19449*, 2024.
- Peihua Li, Jiangtao Xie, Qilong Wang, and Zilin Gao. Towards faster training of global covariance pooling networks by iterative matrix square root normalization. In *Proceedings of the IEEE conference on computer vision and pattern recognition*, pp. 947–955, 2018.

- Vladislav Lialin, Namrata Shivagunde, Sherin Muckatira, and Anna Rumshisky. Relora: High-rank training through low-rank updates. In *International Conference on Learning Representations*, 2023. URL <https://api.semanticscholar.org/CorpusID:259836974>.
- Hong Liu, Zhiyuan Li, David Hall, Percy Liang, and Tengyu Ma. Sophia: A scalable stochastic second-order optimizer for language model pre-training. *CoRR*, abs/2305.14342, 2023.
- Ilya Loshchilov and Frank Hutter. Decoupled weight decay regularization. In *ICLR (Poster)*. OpenReview.net, 2019.
- Igor Molybog, Peter Albert, Moya Chen, Zachary DeVito, David Esiobu, Naman Goyal, Punit Singh Koura, Sharan Narang, Andrew Poulton, Ruan Silva, et al. A theory on adam instability in large-scale machine learning. *arXiv preprint arXiv:2304.09871*, 2023.
- Yurii Nesterov. *Introductory lectures on convex optimization: A basic course*, volume 87. Springer Science & Business Media, 2013.
- Matteo Pagliardini, Pierre Ablin, and David Grangier. The ademamix optimizer: Better, faster, older. *arXiv preprint arXiv:2409.03137*, 2024.
- Colin Raffel, Noam Shazeer, Adam Roberts, Katherine Lee, Sharan Narang, Michael Matena, Yanqi Zhou, Wei Li, and Peter J. Liu. Exploring the limits of transfer learning with a unified text-to-text transformer. *Journal of Machine Learning Research*, 21(140):1–67, 2020. URL <http://jmlr.org/papers/v21/20-074.html>.
- Noam Shazeer and Mitchell Stern. Adafactor: Adaptive learning rates with sublinear memory cost. In *ICML*, volume 80 of *Proceedings of Machine Learning Research*, pp. 4603–4611. PMLR, 2018.
- Yuandong Tian, Yiping Wang, Zhenyu Zhang, Beidi Chen, and Simon Du. Joma: Demystifying multilayer transformers via joint dynamics of mlp and attention. *arXiv preprint arXiv:2310.00535*, 2023.
- Tijmen Tieleman. Lecture 6.5-rmsprop: Divide the gradient by a running average of its recent magnitude. *COURSERA: Neural networks for machine learning*, 4(2):26, 2012.
- Hugo Touvron, Louis Martin, Kevin Stone, Peter Albert, Amjad Almahairi, Yasmine Babaei, Nikolay Bashlykov, Soumya Batra, Prajjwal Bhargava, Shruti Bhosale, Dan Bikel, Lukas Blecher, Cristian Canton Ferrer, Moya Chen, Guillem Cucurull, David Esiobu, Jude Fernandes, Jeremy Fu, Wenyin Fu, Brian Fuller, Cynthia Gao, Vedanuj Goswami, Naman Goyal, Anthony Hartshorn, Saghar Hosseini, Rui Hou, Hakan Inan, Marcin Kardas, Viktor Kerkez, Madian Khabsa, Isabel Kloumann, Artem Korenev, Punit Singh Koura, Marie-Anne Lachaux, Thibaut Lavril, Jenya Lee, Diana Liskovich, Yinghai Lu, Yuning Mao, Xavier Martinet, Todor Mihaylov, Pushkar Mishra, Igor Molybog, Yixin Nie, Andrew Poulton, Jeremy Reizenstein, Rashi Rungta, Kalyan Saladi, Alan Schelten, Ruan Silva, Eric Michael Smith, Ranjan Subramanian, Xiaoqing Ellen Tan, Binh Tang, Ross Taylor, Adina Williams, Jian Xiang Kuan, Puxin Xu, Zheng Yan, Iliyan Zarov, Yuchen Zhang, Angela Fan, Melanie Kambadur, Sharan Narang, Aurelien Rodriguez, Robert Stojnic, Sergey Edunov, and Thomas Scialom. Llama 2: Open foundation and fine-tuned chat models, 2023. URL <https://arxiv.org/abs/2307.09288>.
- Jingzhao Zhang, Sai Praneeth Karimireddy, Andreas Veit, Seungyeon Kim, Sashank Reddi, Sanjiv Kumar, and Suvrit Sra. Why are adaptive methods good for attention models? *Advances in Neural Information Processing Systems*, 33:15383–15393, 2020.
- Susan Zhang, Stephen Roller, Naman Goyal, Mikel Artetxe, Moya Chen, Shuohui Chen, Christopher Dewan, Mona Diab, Xian Li, Xi Victoria Lin, et al. Opt: Open pre-trained transformer language models. *arXiv preprint arXiv:2205.01068*, 2022.
- Yushun Zhang, Congliang Chen, Tian Ding, Ziniu Li, Ruoyu Sun, and Zhi-Quan Luo. Why transformers need adam: A hessian perspective. *arXiv preprint arXiv:2402.16788*, 2024.
- Jiawei Zhao, Zhenyu (Allen) Zhang, Beidi Chen, Zhangyang Wang, Anima Anandkumar, and Yuandong Tian. Galore: Memory-efficient llm training by gradient low-rank projection. *ArXiv*, abs/2403.03507, 2024a. URL <https://api.semanticscholar.org/CorpusID:268253596>.

Rosie Zhao, Depen Morwani, David Brandfonbrener, Nikhil Vyas, and Sham Kakade. Deconstructing what makes a good optimizer for language models. *arXiv preprint arXiv:2407.07972*, 2024b.

Zhanxing Zhu, Jingfeng Wu, Bing Yu, Lei Wu, and Jinwen Ma. The anisotropic noise in stochastic gradient descent: Its behavior of escaping from sharp minima and regularization effects. *arXiv preprint arXiv:1803.00195*, 2018.

A DESIRED PROPERTIES OF ADAPTIVE OPTIMIZERS

There is a rich literature on understanding adaptive methods’ inner workings and unreasonable effectiveness. Using Adam as an example, we first summarize from the literature below the key desired properties of stateful adaptive optimizers that contribute to their empirical success: *gradient smoothing*, *gradient invariance*, and *gradient whitening*. Then we discuss how these understandings will lead to the design of *stateless* adaptive optimizers.

Gradient Smoothing. Under the stochastic optimization setting, mini-batch sampling introduces heterogeneous distribution shift on the gradient distribution: $\mathbf{G}^{(t)} = \mathbb{E}[\mathbf{G}^{(t)}] + \varepsilon^{(t)}$, where $\varepsilon^{(t)}$ is time-heterogeneous noise induced by mini-batch sampling. While $\varepsilon^{(t)}$ helps SGD escape local optima (Jastrzębski et al., 2017; Zhu et al., 2018), the *covariate shift* of $\varepsilon^{(t)}$ over time also presents challenges to learning as the model needs to adjust and compensate for this shift, especially under the emergence of heavy-tailed gradient distributions (Zhang et al., 2020)⁵. Following this viewpoint, it has been proven that momentum reduces the influence of noises for SGD (Cutkosky & Mehta, 2020; Crawshaw et al., 2022). Therefore we hypothesize that the first moment estimate $\mathbf{m}^{(t)}$ of Adam also effectively stabilizes gradient distribution and reduces effect of $\varepsilon^{(t)}$. This smoothing stabilizes the variance caused by noisy stochastic gradients across time.

Gradient Invariance. More recently it has also been identified (Kunstner et al., 2023; 2024) that the major factor contributing to the performance gap between SGD and Adam might lie in Adam’s *Sign-descent*-like nature (Bernstein et al., 2018; Crawshaw et al., 2022; Chen et al., 2023). Intuitively, Adam without bias correction under $\beta_1 = 0$ and $\beta_2 = 0$ is equivalent to signed gradient descent ($\Delta\mathbf{W} = \text{sign}(\mathbf{G})$). Indeed, the performance of Adam can be closely reproduced (Kunstner et al., 2023; Crawshaw et al., 2022) or even surpassed (Chen et al., 2023) by variants of signed descent with momentum. Apart from sign-based methods, evidence on performance boost using gradient clipping/normalization was also discussed in the context of understanding Adam (Zhang et al., 2020). Therefore, we hypothesize that one of the key properties of Adam is that it offers *invariance over certain transformations on gradients*. Particularly, the original Adam is invariant to diagonal rescaling of the gradients (Kingma & Ba, 2015); the signed gradient method is invariant to *any* scaling that preserves the sign of gradients; and the clipped SGD variant is invariant to extreme gradient magnitude spikes.

Gradient Whitening. Finally, we argue that the empirical success of adaptive methods also lies in that they model the curvature by first-order information. This is realized by the second moment estimate $\nu^{(t)}$, which approximates the diagonal of the Fisher information matrix (Kingma & Ba, 2015; Hwang, 2024); helping to counteract local curvatures of the problem. Specifically, Adam computes a trailing estimation of the diagonal coefficients of the Fisher matrix $\mathbf{F} = \mathbb{E}[\mathbf{g}\mathbf{g}^\top]$ by tracking $\hat{\mathbf{F}} = \text{diag}(\mathbf{F}) = \text{diag}[\mathbb{E}[\mathbf{g}^2]]$, where $\mathbf{g} = \text{vec}(\mathbf{G})$ is the vectorized gradient. Interestingly, instead of preconditioning the first moment as $\hat{\mathbf{F}}^{-1}\text{vec}(\mathbf{m})$, Adam uses a whitening-like preconditioned update $\hat{\mathbf{F}}^{-\frac{1}{2}}\text{vec}(\mathbf{m})$, suggesting an *element-wise* approximate whitening of the gradient. It has been shown that such element-wise whitening leads to diagonal approximation to inverse Hessian $\hat{\mathbf{F}}^{-\frac{1}{2}} \approx \text{diag}(\mathbf{H}^{-1})$ (Molybog et al., 2023). Recent empirical studies show that Adam biases optimization trajectories towards regions where the condition number of Hessian is low (Jiang et al., 2024). Therefore, we hypothesize that Adam approximately whitens the gradients element-wise, leading to well-conditioned regions.

B THEORETICAL ANALYSIS

B.1 ANALYZING THE GRADNORM: A TRANSFORMER LEARNING DYNAMICS PERSPECTIVE

We take the transformer LLM architecture as an example, and demonstrate that GradNorm effectively removes the time-variant components of gradient noises. For our analysis, we assume the following

⁵Such shift cannot be removed by forward covariate-shift reduction architectures such as Layer Norm, as it is only invariant to global scaling and re-centering, such as $\mathbf{W}^{(t)} = \delta\mathbf{W}^{(t)} + \gamma\mathbf{1}^\top$ for some scalar δ and incoming vector shift γ (Ba et al., 2016).

simplified transformer block (STB) architecture recently proposed in [Tian et al. \(2023\)](#), which contains the major building blocks of transformers and relies on relatively less restrictive assumptions and simplifications, making them suitable for theoretical analysis for transformer dynamics. It is defined as follows:

Definition 1 (Simplified Transformer Block (STB)). *Given the input activation $\mathbf{x} \in \mathbb{R}^{M_C \times 1}$, query token index q , context embedding matrix $\mathbf{U}_C \in \mathbb{R}^{d \times M_C}$, and the query embedding $\mathbf{u}_q \in \mathbb{R}^{d \times 1}$, the simplified transformer block computes the output $\mathbf{h} \in \mathbb{R}^{n \times 1}$ as follows:*

$$\mathbf{h} = \phi \left(\mathbf{W}^\top (\mathbf{U}_C (\exp(\mathbf{z}_q) \odot \mathbf{x}) + \mathbf{u}_q) \right),$$

where the attention logits $\mathbf{z}_q \in \mathbb{R}^{M_C \times 1}$ are given by

$$z_{ql} = \mathbf{u}_q^\top \mathbf{W}_Q^\top \mathbf{W}_K \mathbf{u}_l,$$

with $\mathbf{W}_Q, \mathbf{W}_K \in \mathbb{R}^{d \times d}$ being weight matrices for the queries and keys, respectively, $\mathbf{W} \in \mathbb{R}^{d \times n}$ is the weight matrix for the feedforward network, and ϕ is a nonlinearity function such as ReLU.

Given a STB, we consider the following standard mini-batch learning dynamics. Define the conditional expectation $\mathbb{E}_{q=m}[\cdot] := \mathbb{E}[\cdot | q = m]$. Consider the dynamics of the weight matrix \mathbf{W} and the attention logits \mathbf{z}_q , if we train the model with a batch of inputs that always end up with query $q[i] = m$. The weight update for \mathbf{W} and \mathbf{z}_q are given by the following noisy updates:

$$\dot{\mathbf{W}}^{(t)} = \mathbb{E}_{q=m} \left[\mathbf{f}^{(t)} (\mathbf{G}_h \odot \mathbf{h}'^{(t)})^\top \right] + \boldsymbol{\varepsilon}^{(t)}, \quad \dot{\mathbf{z}}_m^{(t)} = \mathbb{E}_{q=m} \left[\left(\frac{\partial \mathbf{b}}{\partial \mathbf{z}_m^{(t)}} \right)^\top \mathbf{U}_C^\top \mathbf{g}_f^{(t)} \right] + \boldsymbol{\varsigma}^{(t)}, \quad (10)$$

Where $\mathbf{f}^{(t)} = \left(\mathbf{U}_C (\exp(\mathbf{z}_q^{(t)}) \odot \mathbf{x}) + \mathbf{u}_q \right)$, $(\mathbf{h}^{(t)})' = \phi'((\mathbf{W}^{(t)})^\top \mathbf{f}^{(t)})$ is the derivative of the current activation, $\mathbf{G}_h^{(t)} = \nabla_{\mathbf{h}^{(t)}} \mathcal{L}$ is the gradient of the loss function \mathcal{L} with respect to the hidden activation $\mathbf{h}^{(t)}$, and $\mathbf{g}_{\mathbf{f}^{(t)}}^{(t)} = \sum_k \mathbf{g}_{\mathbf{h}_k^{(t)}}^{(t)} (\mathbf{h}_k^{(t)})' \mathbf{w}_k^{(t)}$ is the sum of the gradients with respect to the attention logits. Here, $\mathbf{w}_k^{(t)}$ is the k -th column of $\mathbf{W}^{(t)}$, $\mathbf{g}_{\mathbf{h}_k^{(t)}}^{(t)}[i]$ be the backpropagated gradient sent to node k at sample i . Finally, $\boldsymbol{\varepsilon}$ and $\boldsymbol{\varsigma}$ are random noises that are induced by the minibatch sampling.

Remark Given STB under the dynamics of Equation (10), the distribution of noises $\boldsymbol{\varepsilon}^{(t)}$ and $\boldsymbol{\varsigma}^{(t)}$ generally vary across time, since both the integrand within expectation, $\mathbf{f}^{(t)} (\mathbf{G}_h \odot \mathbf{h}'^{(t)})^\top$ and $\left(\frac{\partial \mathbf{b}}{\partial \mathbf{z}_m^{(t)}} \right)^\top \mathbf{U}_C^\top \mathbf{g}_f^{(t)}$ vary across time. However, the following result on GradNorm suggests that this time variability of $\boldsymbol{\varepsilon}^{(t)}$ and $\boldsymbol{\varsigma}^{(t)}$ are completely removed by GradNorm:

Theorem 1 (GradNorm stabilizes gradient distribution across time for STB). *Consider the STB (Definition 1). Assuming we inherit the assumptions in Theorem 1 of [Tian et al. \(2023\)](#), as described in Appendix B. Then consider $\mathbf{U}_C^\top \mathbf{W}$, the composition of the MLP project-up matrix and the embedding matrix as a whole. Then, its standardized stochastic gradients $\tilde{\mathbf{G}}_{\mathbf{U}_C^\top \mathbf{W}}^{(t)} := \text{GradNorm} \left(\frac{\partial \mathcal{L}_{\mathbf{w}, \mathbf{z}}(\top \mathbf{x}^{(t)})}{\mathbf{U}_C^\top \mathbf{W}} \right)$ satisfy:*

$$\text{Cov}[\tilde{\mathbf{G}}_{\mathbf{U}_C^\top \mathbf{W}}[i, :]^{(t_1)}] = \text{Cov}[\tilde{\mathbf{G}}_{\mathbf{U}_C^\top \mathbf{W}}[i, :]^{(t_2)}] \quad \text{for all } t_1, t_2, \text{ and } i.$$

In other words, the covariance structure of $\tilde{\mathbf{G}}$ is identical across all time steps t , achieving distributional stability across time. The same relationship also holds for the gradient of attention score $\tilde{\mathbf{G}}_{\mathbf{z}_q}^{(t)} := \text{GradNorm} \left(\frac{\partial \mathcal{L}_{\mathbf{w}, \mathbf{z}_q}(\top \mathbf{x}^{(t)})}{\partial \mathbf{z}_q} \right)$.

Theorem 1 suggests that GradNorm makes use of the inductive bias induced by transformer architectures and directly removes the time-variant components in gradient covariance structures caused by mini-batch sampling. In practice, GradNorm makes the following approximation to Theorem 1: For MLP layer GradNorm is applied on \mathbf{W} instead of $\mathbf{U}_C^\top \mathbf{W}$ as a whole, since such grouping does not exist in practical transformer architectures. However, it still works reasonably well in practice (Section 5, Section 5.6).

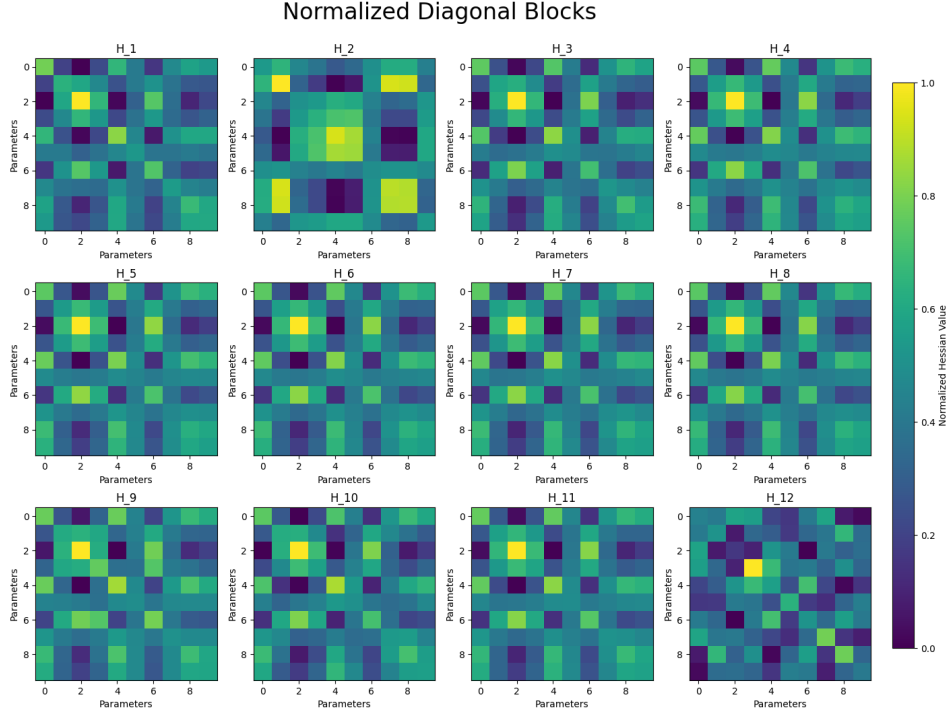


Figure 9: Normalized Hessian Blocks of size $M_C \times M_C$ along the diagonal direction of the Hessian, obtained from numerically solving the STB ODE (with $n = 12$, $M_C = 10$) (1) given by the full-batch dynamics (i.e., removing noise in Equation (10)). During all training steps, we analytically track the evolution of Hessian. As predicted by Proposition 1, we see very similar structures across the diagonal blocks of the Hessian.

B.2 ANALYZING GRADWHITENING PT. I: A TRANSFORMER LEARNING DYNAMICS PERSPECTIVE

In this section, we take the perspective of transformer learning dynamics, and show that how GradWhitening can be naturally derived from the simplified transformer model defined in Definition 1.

Let us first consider the dynamics of the Hessian matrix of STB. We will show that: i), it turns out that at equilibrium, the Hessian is highly structured; ii), under some conditions, GradWhitening recovers Newton’s method-like behaviors under such Hessian structures. Below we first present the following result on the Hessian structure of the simplified transformer block at equilibrium:

Proposition 1 (Shared structures in the block-diagonal of Hessians at transformer equilibrium). Consider a STB (1), trained by full-batch dynamics (i.e., removing noise in Equation (10)). Assume we inherit all the assumptions from Theorem 1 of Tian et al. (2023). Consider the following Hessian matrix:

$$\mathbf{H}(\mathbf{W})_{sk,s'k'} = \frac{\partial \mathcal{L}}{\partial w_{sk} \partial w_{s'k'}}$$

where $1 \leq s, s' \leq m$, $1 \leq k, k' \leq n$. Then, as $t \rightarrow \infty$, we have the following shared Hessian structure along the diagonal blocks:

$$\frac{\mathbf{H}_{sk,s'k}}{\sum_{s,s'} \mathbf{H}_{sk,s'k}} \rightarrow \frac{\mathbf{H}_{sk',s'k'}}{\sum_{s,s'} \mathbf{H}_{sk',s'k'}}, \quad \forall 1 \leq s, s' \leq d, 1 \leq k, k' \leq n \quad (11)$$

Proposition 1 shows that, under a simplified setting of transformer, because of the winner-takes-all behavior in the attention model, the Hessian will also converge to an equilibrium solution where the $M_C \times M_C$ blocks over the diagonal direction of Hessian shares the identical structure, after normalization. This result is verified in our numerical experiment as shown in Figure 9.

Given by the inductive bias that equality across diagonal blocks of Hessians at transformer learning equilibrium, in the next theorem we show that GradWhitening can be derived as a second-order method under this structural assumption

Theorem 2 (GradWhitening as structural approximation of Hessian). *Consider the optimization problem given by $\min_{\mathbf{W} \in \mathbb{R}^{m \times n}} f(\mathbf{W})$ where $\mathbf{W} \in \mathbb{R}^{m \times n}$, with $m < n$. Assume:*

- *The local Hessian H of f has shared block-diagonal, such that $\mathbf{H} = \text{diag}(\tilde{\mathbf{H}}, \tilde{\mathbf{H}}, \dots, \tilde{\mathbf{H}}, \dots, \tilde{\mathbf{H}}) = \mathbf{I}_{n \times n} \otimes \tilde{\mathbf{H}}$, where $\tilde{\mathbf{H}} \in \mathbb{R}^{m \times m}$.*
- *$\mathbf{W}^{(t)}$ is initialized as a orthogonal matrix.*

Then (under 2nd order approximation) GradWhitening’s modified gradient descent (Equation (13)) on f recovers the update of Newton’s method, without explicitly estimate second-order quantities.

To summarize, GradWhitening recovers a Newton’s method-like behavior under the highly structured Hessian regime (i.e., there exists $\tilde{\mathbf{H}}$ such that $\mathbf{H} = \mathbf{I}_{n \times n} \otimes \tilde{\mathbf{H}}$), which is partially satisfied in transformer equilibrium dynamics (see remark below). Compared to directly applying accelerated second-order methods such as the Gauss-Newton method ($\mathcal{O}(Bm^2n^2 + m^3n^3)$, B being batch size) or conjugate gradient method ($\mathcal{O}(BTmn)$ complexity, $T = 10 \sim 100$, with worst case complexity $\mathcal{O}(Bm^2n^2)$), GradWhitening should be much faster ($\mathcal{O}(mn \min\{m, n\})$), especially under the Newton-Schulz iteration.

Remark: limitations Proposition 1 deviates from the strict assumptions of Theorem 2 in that: Proposition 1 only asserts that diagonal direction of Hessian shares the identical structure, but does not assert that the *off-diagonal* blocks are zero, without further assumptions on g_{h_k} . However, given that it is standard practice to ignore off-diagonal *elements* in many practical optimizers including Adam, we hereby argue that ignoring off-diagonal *blocks* is already a better approximation.

B.3 ANALYZING THE GRADWHITENING PT. II: ROBUSTNESS AGAINST LOCAL CURVATURE

In this section, we present main results regarding the convergence rate of the GradWhitening method, understand its implications, and compare it with the lower bounds of GD and Adam.

First, for simplicity, we focus on the following quadratic problem:

$$\mathcal{L}(\mathbf{W}) = \frac{1}{2} \text{Tr}(\mathbf{W}^\top \mathbf{H} \mathbf{W}) - \text{Tr}(\mathbf{C}^\top \mathbf{W}), \quad (12)$$

where $\mathbf{W} \in \mathbb{R}^{m \times n}$ is the parameter matrix, $\mathbf{H} \in \mathbb{R}^{m \times m}$ is a positive definite matrix, and $\mathbf{C} \in \mathbb{R}^{m \times n}$ is a constant matrix.

For simplicity and without loss of generality, we assume $\mathbf{C} = 0$. This is because minimizing $\mathcal{L}(\mathbf{W}) = \frac{1}{2} \text{Tr}(\mathbf{W}^\top \mathbf{H} \mathbf{W}) - \text{Tr}(\mathbf{C}^\top \mathbf{W})$ is equivalent to minimizing $\mathcal{L}(\mathbf{W}) = \frac{1}{2} \text{Tr}[(\mathbf{W} - \mathbf{W}^*)^\top \mathbf{H} (\mathbf{W} - \mathbf{W}^*)]$, where $\mathbf{W}^* = \mathbf{H}^{-1} \mathbf{C}$. By defining $\mathbf{Z} = \mathbf{W} - \mathbf{W}^*$, the problem reduces to minimizing $\mathcal{L}(\mathbf{Z}) = \frac{1}{2} \text{Tr}(\mathbf{Z}^\top \mathbf{H} \mathbf{Z})$.

Remark Most results in this note can be easily extended to any loss function that are either i) strongly convex; or ii) has twice differentiable functions and Lipschitz continuous Hessian, by considering their the second order approximation around \mathbf{W}^* .

Next, to understand the effect of GradWhitening, we will examine the gradient flow dynamics induced by GradWhitening. Consider the GradWhitening-modified gradient descent:

$$\Delta \mathbf{W}^{(t)} = -\eta \text{GradWhitening}(\mathbf{G}^{(t)}) \quad (13)$$

its exact convergence rate is given by the result as below:

Theorem 3 (Contraction factor of GradWhitening). *Consider the quadratic loss function Equation (12). Assume the initialization distribution of \mathbf{W}^0 assigns zero probability to any set of zero Lebesgue measure in $\mathbb{R}^{m \times n}$. Let our update rule be:*

$$\mathbf{W}_{\text{whitened}}^{(t+1)} = \mathbf{W}_{\text{whitened}}^{(t)} - \eta \text{GradWhitening}(\mathbf{G}^{(t)})$$

where the learning rate is η . Then, with probability 1, we have:

- The optimal dynamic learning rate to achieve the fastest convergence is given by

$$\eta^{(t)*} = \frac{\|\mathbf{HW}_{\text{whitened}}^{(t)}\|_1}{\text{Tr}[\mathbf{H}]} \quad (14)$$

where $\|\mathbf{HW}_{\text{whitened}}^{(t)}\|_1$ denotes the Schatten p -norm with $p = 1$ (i.e., sum of singular values).

- Under $\eta^{(t)*}$, the contraction factor of loss function at t is given by:

$$\frac{\mathcal{L}(\mathbf{W}_{\text{whitened}}^{(t+1)}) - \mathcal{L}^*}{\mathcal{L}(\mathbf{W}_{\text{whitened}}^{(t)}) - \mathcal{L}^*} = 1 - \frac{\|\mathbf{HW}_{\text{whitened}}^{(t)}\|_1^2}{\text{Tr}[(\mathbf{W}_{\text{whitened}}^{(t)})^\top \mathbf{HW}_{\text{whitened}}^{(t)}] \text{Tr}[\mathbf{H}]} \quad (15)$$

- Furthermore, if we additionally enforce $\mathbf{W}^0 \sim V^{m \times n}(\mathbb{R})$, i.e., initialized as an element in Stiefel manifold. Then we have

$$\frac{\mathcal{L}(\mathbf{W}_{\text{whitened}}^{t=1}) - \mathcal{L}^*}{\mathcal{L}(\mathbf{W}^0) - \mathcal{L}^*} = 0 \quad (16)$$

That is, GradWhitening solves the optimization problem (Equation (12)) with 1 step iteration.

Theorem 3 has the following key implications.

Convergence rate is condition number agnostic Unlike the convergence rates of GD and Adam presented in Zhang et al. (2024), as well as Theorem 4 and Corollary 1 in Appendix, the optimal convergence rate (15) of GradWhitening no longer explicitly depends on the condition number κ of H . In fact, consider a lower bound $\frac{\|\mathbf{HW}_{\text{whitened}}^{(t)}\|_1^2}{\text{Tr}[(\mathbf{W}_{\text{whitened}}^{(t)})^\top \mathbf{HW}_{\text{whitened}}^{(t)}] \text{Tr}[\mathbf{H}]} \geq \frac{\text{Tr}[\mathbf{HW}_{\text{whitened}}^{(t)}]^2}{\text{Tr}[(\mathbf{W}_{\text{whitened}}^{(t)})^\top \mathbf{HW}_{\text{whitened}}^{(t)}] \text{Tr}[\mathbf{H}]}$, since trace of H appear both in the nominator and denominator, we expect that to be more robust to ill-conditioned problems. For example, consider the specific initialization $\mathbf{W}_{\text{whitened}}^{(t)} = cI$, it is straightforward to show that $\frac{\|\mathbf{HW}_{\text{whitened}}^{(t)}\|_1^2}{\text{Tr}[(\mathbf{W}_{\text{whitened}}^{(t)})^\top \mathbf{HW}_{\text{whitened}}^{(t)}] \text{Tr}[\mathbf{H}]} \geq \frac{\text{Tr}[\mathbf{HW}_{\text{whitened}}^{(t)}]^2}{\text{Tr}[(\mathbf{W}_{\text{whitened}}^{(t)})^\top \mathbf{HW}_{\text{whitened}}^{(t)}] \text{Tr}[\mathbf{H}]} \perp \kappa$, which is completely disentangled from the condition number. Hence $\frac{\|\mathbf{HW}_{\text{whitened}}^{(t)}\|_1^2}{\text{Tr}[(\mathbf{W}_{\text{whitened}}^{(t)})^\top \mathbf{HW}_{\text{whitened}}^{(t)}] \text{Tr}[\mathbf{H}]}$ would not shrink as $\kappa \rightarrow \infty$. See Proposition 2 for less extreme situations.

Superlinear convergence with Stiefel manifold initialization Theorem 3 suggests that if $\mathbf{W}_{\text{whitened}}^{(t)}$ is initialized in the Stiefel manifold, then GradWhitening reaches superlinear convergence rate (= Newton's method), while being cheaper. In fact, it is straightforward to verify that GradWhitening reaches optimal solution with 1 step update. This implies GradWhitening is theoretically the optimal optimization algorithm if \mathbf{W} is initialized in the Stiefel manifold.

Estimation and interpretation of optimal learning rate Compared to the optimal dynamic learning rate of gradient descent $G = \frac{G^\top G}{G^\top H G}$, the optimal learning rate $\eta^{(t)*}$ of GradWhitening is much easier to compute. $\frac{\text{Tr}[\mathbf{HW}_{\text{whitened}}^{(t)}]}{\text{Tr}[\mathbf{H}]}$ can be seen as balancing the average gradient magnitude against the average curvature. A higher trace of gradient ($\mathbf{HW}_{\text{whitened}}^{(t)}$) (strong gradients) relative to \mathbf{H} (steep curvature) suggests a larger learning rate, promoting faster updates. Conversely, a higher trace of \mathbf{H} would imply a smaller learning rate to ensure stable convergence in regions with high curvature.

Next, we show that the convergence speed of GradWhitening update is indeed robust to the condition number of local curvature.

Proposition 2 (Robustness of GradWhitening update convergence rate against the condition number of local Hessian). Consider the quantity:

$$Q := \frac{\text{Tr}[\mathbf{HW}_{\text{whitened}}^t]^2}{\text{Tr}[(\mathbf{W}_{\text{whitened}}^{(t)})^\top \mathbf{HW}_{\text{whitened}}^{(t)}] \text{Tr}[\mathbf{H}]}$$

Assume: i), $\mathbf{W}_{\text{whitened}}^{(t)} \neq \mathbf{W}^*$; and ii) the norm of \mathbf{H} is bounded. Then, there exist some finite positive constant c , such that

$$Q > c$$

This holds even if $\kappa \rightarrow +\infty$, where κ is the condition number of \mathbf{H} .

Below, we provide comparison between GradWhitening modified gradient descent and Adam. We only consider non-Stiefel initialization for GradWhitening, since with non-Stiefel initialization GradWhitening is optimal according to Theorem 3. Our results below shows that, for poor conditioned problems GradWhitening with a properly chosen single global learning rate always outperforms Adam even with *optimally tuned sub-group learning rates*, in terms of convergence speed.

Proposition 3 (GradWhitening with single lr vs Adam with tuned group lr). *Consider the optimization problem Equation (12). Assume \mathbf{H} is block-diagonal, i.e., $\mathbf{H} = \text{diag}(\mathbf{H}_1, \mathbf{H}_2, \dots, \mathbf{H}_L)$, where each $\mathbf{H}_l \in \mathbb{R}^{m_l \times m_l}$ is a positive definite matrix for $l = 1, 2, \dots, L$, and $\sum_{l=1}^L m_l = m$. Assuming for GradWhitening we use one global learning rate for all parameters; and for Adam, we use the optimally chosen group learning rate η_l and initial condition w_0 for each block \mathbf{H}_l .*

Assume either if i) certain regularity conditions are met (see proof in Appendix), or ii), if \mathbf{H} is poorly-conditioned (its condition number is large enough). Then: regardless of its initialization, GradWhitening with a properly chosen learning rate will still have a strictly better convergence speed (i.e., smaller contraction factor) across all blocks $l \in [L]$ than Adam ($\beta_1 = 0, \beta_2 = 1$) under optimal group-wise learning rates and initial condition.

Remark As pointed out by Zhang et al. (2024) and Da Silva & Gazeau (2020), Adam with $\beta_2 < 1$ will have issues with convergence, which will not be completely removed even with lr decay. Therefore, we will not discuss the case of $\beta_2 < 1$ to avoid the complication.

Proposition 3 confirmed our claim in Section 3 that SWAN is *not* an approximation to Adam; and in the scenarios claimed by Proposition 3, the GradWhitening-induced weight update rule has strictly faster convergence compared with Adam, even the Adam global learning rate is tuned per-group wise.

C PROOF OF THEOREM 1

Proof. We first consider the noiseless, full batch dynamics. Define $\mathbf{V} \in \mathbb{R}^{M_C \times n}$ as $\mathbf{V} := \mathbf{U}_C^\top \mathbf{W}$. Then following Theorem 2 in Tian et al. (2023), each column of \mathbf{V} satisfies the following differential equation:

$$\dot{\mathbf{V}}_{[:,j]} = \exp(\mathbf{V}_{[:,j]}^2/2 + C) \odot \mathbb{E}_q[g_{h_j} \mathbf{x}] \quad (17)$$

The corresponding dynamics of attention score is given by:

$$\mathbf{z}_q = \frac{1}{2} \sum_j \mathbf{V}_{[:,j]}^2. \quad (18)$$

Without loss of generality, in this proof we only consider $C = 0$.

Now, following the argument of Lemma B.6 of Zhao et al. (2024a), we reparameterize the dynamics *row-wise*. For this, consider instead

$$\mathbf{V} = \begin{bmatrix} \mathbf{u}_1^\top \\ \mathbf{u}_2^\top \\ \vdots \\ \mathbf{u}_{M_C}^\top \end{bmatrix}$$

Then, equation 17 becomes:

$$\dot{\mathbf{u}}_i = [\exp(\mathbf{u}_i^2) \cdot \mathbf{1}] \boldsymbol{\mu}_i \quad (19)$$

where $\boldsymbol{\mu}_i \in \mathbb{R}^{n \times 1}$ is given by $[\boldsymbol{\mu}_i]_j := \mathbb{E}_q[g_{h_j} x_i]$. Therefore, it is clear that \mathbf{u}_i always move along the direction of $\boldsymbol{\mu}_i$ due to the stationary back-propagated gradient assumption. Hence, $\dot{\mathbf{u}}_i = \alpha_i(t) \boldsymbol{\mu}_i$ for some scalar dynamics $\alpha_i(t)$.

Next, consider the mini-batch version of the dynamics. In this case, the backpropagated gradient term $[\boldsymbol{\mu}_i]_j := \mathbb{E}_q[g_{h_j} x_i]$ is corrupted by some i.i.d. mini-batch noise $\boldsymbol{\xi}$. The noisy row-wise dynamics now becomes:

$$\dot{\mathbf{u}}_i = \alpha_i(t)(\boldsymbol{\mu}_i + \boldsymbol{\xi}_i) \quad (20)$$

Therefore, after row-wise standardization, the new dynamics becomes

$$\begin{aligned} \dot{\hat{\mathbf{u}}}_i &= \frac{\alpha_i(t)(\boldsymbol{\mu}_i + \boldsymbol{\xi}_i) - \alpha_i(t)\left(\frac{1}{n}\sum_j \mu_{ij} + \frac{1}{n}\sum_j \xi_{ij}\right)}{\alpha_i(t)\left(\frac{1}{n}\sum_j (\mu_{ij} + \xi_{ij} - \frac{1}{n}\sum_j \mu_{ij} - \frac{1}{n}\sum_j \xi_{ij})^2\right)} \\ &= \frac{(\boldsymbol{\mu}_i + \boldsymbol{\xi}_i) - \left(\frac{1}{n}\sum_j \mu_{ij} + \frac{1}{n}\sum_j \xi_{ij}\right)}{\left(\frac{1}{n}\sum_j (\mu_{ij} + \xi_{ij} - \frac{1}{n}\sum_j \mu_{ij} - \frac{1}{n}\sum_j \xi_{ij})^2\right)} \end{aligned}$$

Therefore, the normalized noisy gradient $\dot{\hat{\mathbf{u}}}_i$ no longer depend on the time-variant component $\alpha(t)$. Hence, we have proved:

$$\text{Cov}[\tilde{\mathbf{G}}_{\mathbf{U}^\top \mathbf{W}}[i, :](^{t_1})] = \text{Cov}[\tilde{\mathbf{G}}_{\mathbf{U}^\top \mathbf{W}}[i, :](^{t_2})] \quad \text{for all } t_1, t_2, \text{ and } i.$$

The corresponding result for $\tilde{\mathbf{G}}_{\mathbf{z}_q}^{(t)} := \text{GradNorm}\left(\frac{\partial \mathcal{L}_{\mathbf{W}, \mathbf{z}_q}(\top \mathbf{x}^{(t)})}{\mathbf{z}_q}\right)$ can be trivially derived due to Equation (18). \square

D PROOF OF THEOREM 3

Proof. We first show that $\nabla \mathcal{L}(\mathbf{W}^{(0)}) = \mathbf{H}\mathbf{W}^{(0)}$ (and hence $\nabla \mathcal{L}(\mathbf{W}_{\text{whitened}}^{(t)})$ with $t \neq \infty$) are non-zero with probability 1 under Assumption of the theorem. Given $\nabla \mathcal{L}(\mathbf{W}^{(0)}) = \mathbf{H}\mathbf{W}^{(0)}$, the set of matrices $\mathbf{W}^{(0)}$ such that $\text{Tr}(\mathbf{H}\mathbf{W}^{(0)}) = 0$ forms a hyperplane in the space of $d \times d$ matrices. Specifically, it is defined by the linear equation: $\text{Tr}(\mathbf{H}\mathbf{W}^{(0)}) = 0$. Since \mathbf{H} is positive definite, at least one entry of \mathbf{H} is non-zero. Thus, the hyperplane $\text{Tr}(\mathbf{H}\mathbf{W}^{(0)}) = 0$ has zero Lebesgue measure in the space of $d \times d$ matrices. Given that $\mathbf{W}^{(0)}$ is sampled from a continuous distribution, the probability that $\text{Tr}(\mathbf{H}\mathbf{W}^{(0)}) = 0$ is zero. Therefore, $\nabla \mathcal{L}(\mathbf{W}^{(0)}) \neq 0$ (and hence $\nabla \mathcal{L}(\mathbf{W}_{\text{whitened}}^{(t)})$ with $t \neq \infty$) with probability 1.

Next, we define the cost-to-go as:

$$\mathcal{L}(\mathbf{W}^{(t)}) - \mathcal{L}^* = \frac{1}{2} \text{Tr} \left[(\mathbf{W}^{(t)})^\top \mathbf{H} \mathbf{W}^{(t)} \right],$$

and the per-step improvement is (since $\mathcal{L}^* = 0$ under $\mathbf{W} = 0$),

$$\mathcal{L}(\mathbf{W}^{(t)}) - \mathcal{L}(\mathbf{W}^{(t+1)}) = \frac{1}{2} \text{Tr} \left[(\mathbf{W}^{(t)})^\top \mathbf{H} \mathbf{W}^{(t)} \right] - \frac{1}{2} \text{Tr} \left[(\mathbf{W}^{(t+1)})^\top \mathbf{H} \mathbf{W}^{(t+1)} \right].$$

Substituting the update rule $\mathbf{W}^{(t+1)} = \mathbf{W}^{(t)} - \eta \text{GradWhitening}(\mathbf{G}_{\text{whitened}, l}) = \mathbf{W}^{(t)} - \eta \mathbf{U}\mathbf{V}^\top$, we get:

$$\mathcal{L}(\mathbf{W}^{(t)}) - \mathcal{L}(\mathbf{W}^{(t+1)}) = \frac{1}{2} \text{Tr} \left[(\mathbf{W}^{(t)})^\top \mathbf{H} \mathbf{W}^{(t)} \right] - \frac{1}{2} \text{Tr} \left[(\mathbf{W}^{(t)} - \eta \mathbf{U}\mathbf{V}^\top)^\top \mathbf{H} (\mathbf{W}^{(t)} - \eta \mathbf{U}\mathbf{V}^\top) \right].$$

Expanding the right-hand side, we have

$$\mathcal{L}(\mathbf{W}^{(t)}) - \mathcal{L}(\mathbf{W}^{(t+1)}) = \eta \text{Tr} \left[(\mathbf{W}^{(t)})^\top \mathbf{H} \mathbf{U} \mathbf{V}^\top \right] - \frac{\eta^2}{2} \text{Tr} \left[(\mathbf{U} \mathbf{V}^\top)^\top \mathbf{H} (\mathbf{U} \mathbf{V}^\top) \right].$$

Now, noticing that $\mathbf{G} = \mathbf{H}\mathbf{W}^{(t)} = \mathbf{U}\boldsymbol{\Sigma}\mathbf{V}^\top$, we have:

$$\text{Tr} \left[(\mathbf{W}^{(t)})^\top \mathbf{H} \mathbf{U} \mathbf{V}^\top \right] = \text{Tr} \left[(\mathbf{H}\mathbf{W}^{(t)})^\top \mathbf{U} \mathbf{V}^\top \right] = \text{Tr} \left[(\mathbf{U}\boldsymbol{\Sigma}\mathbf{V}^\top)^\top \mathbf{U} \mathbf{V}^\top \right] = \text{Tr} \left[\mathbf{V}\boldsymbol{\Sigma}\mathbf{U}^\top \mathbf{U} \mathbf{V}^\top \right] = \text{Tr} \left[\mathbf{V}\boldsymbol{\Sigma}\mathbf{V}^\top \right].$$

Since \mathbf{V} is orthogonal, $\mathbf{V}^\top \mathbf{V} = \mathbf{I}$, and Σ is diagonal, we obtain:

$$\text{Tr} \left[(\mathbf{W}^{(t)})^\top \mathbf{H} \mathbf{U} \mathbf{V}^\top \right] = \text{Tr}(\Sigma) = \|\mathbf{H} \mathbf{W}_{\text{whitened}}^{(t)}\|_1.$$

Similarly:

$$\text{Tr} \left[(\mathbf{U} \mathbf{V}^\top)^\top \mathbf{H} (\mathbf{U} \mathbf{V}^\top) \right] = \text{Tr} \left[\mathbf{V} \mathbf{U}^\top \mathbf{H} \mathbf{U} \mathbf{V}^\top \right] = \text{Tr} \left[\mathbf{V} \Lambda \mathbf{V}^\top \right] = \text{Tr}(\mathbf{H}),$$

where Λ is the eigenvalue matrix of \mathbf{H} . Given those intermediate results, we have:

$$\begin{aligned} \frac{\mathcal{L}(\mathbf{W}^{(t+1)}) - \mathcal{L}^*}{\mathcal{L}(\mathbf{W}^{(t)}) - \mathcal{L}^*} &= 1 - \frac{\mathcal{L}(\mathbf{W}^{(t)}) - \mathcal{L}(\mathbf{W}^{(t+1)})}{\mathcal{L}(\mathbf{W}^{(t)}) - \mathcal{L}^*} \\ &= 1 - \frac{\eta \|\mathbf{H} \mathbf{W}_{\text{whitened}}^{(t)}\|_1 - \frac{\eta^2}{2} \text{Tr}(\mathbf{H})}{\frac{1}{2} \text{Tr} \left[(\mathbf{W}^{(t)})^\top \mathbf{H} \mathbf{W}^{(t)} \right]}. \end{aligned}$$

Noticing that this is a quadratic function of η and the second order coefficient is positive, it is straightforward to verify via the quadratic formula that the optimal learning rate is given by

$$\eta_t^* = \frac{\|\mathbf{H} \mathbf{W}_{\text{whitened}}^{(t)}\|_1}{\text{Tr}(\mathbf{H})}.$$

Under which the optimal contraction factor is given by

$$\frac{\mathcal{L}(\mathbf{W}_{\text{whitened}}^{(t+1)}) - \mathcal{L}^*}{\mathcal{L}(\mathbf{W}_{\text{whitened}}^{(t)}) - \mathcal{L}^*} = 1 - \frac{\|\mathbf{H} \mathbf{W}_{\text{whitened}}^{(t)}\|_1^2}{\text{Tr} \left[(\mathbf{W}_{\text{whitened}}^{(t)})^\top \mathbf{H} \mathbf{W}_{\text{whitened}}^{(t)} \right] \text{Tr}(\mathbf{H})}.$$

Finally, if we additionally enforce $\mathbf{W}^{(0)} \sim V^{m \times n}(\mathbb{R})$, i.e., we can parameterize $\mathbf{W}^{(0)} = \mathbf{O}$ where \mathbf{O} is orthogonal, then it is trivial to verify that `GradWhitening` reaches the optimal solution with a 1-step update. To see this, consider the `GradWhitening` update:

$$\mathbf{W}_{\text{whitened}}^{(1)} = \mathbf{O} - \eta^* \mathcal{P}(\mathbf{H} \mathbf{O}) = \mathbf{O} - \frac{\|\mathbf{H} \mathbf{O}\|_1}{\text{Tr}(\mathbf{H})} \mathcal{P}(\mathbf{H} \mathbf{O}),$$

noticing that $\frac{\|\mathbf{H} \mathbf{O}\|_1}{\text{Tr}(\mathbf{H})} = 1$, and $\mathcal{P}(\mathbf{H} \mathbf{O}) = \mathcal{P}(\mathbf{Q} \Lambda \mathbf{Q}^\top \mathbf{O}) = \mathbf{Q} \mathbf{Q}^\top \mathbf{O} = \mathbf{O}$. Hence:

$$\mathbf{W}_{\text{whitened}}^{(1)} = \mathbf{O} - \eta^* \mathcal{P}(\mathbf{H} \mathbf{O}) = \mathbf{O} - \mathbf{O} = \mathbf{0} = \mathbf{W}^*.$$

Hence, the proof is complete. \square

E PROOF OF PROPOSITION 2

Proof. Since $\mathbf{W}_{\text{whitened}}^{(t)} \neq \mathbf{W}^*$, the square of the trace of the gradient $\text{Tr}[\mathbf{H} \mathbf{W}_{\text{whitened}}^{(t)}]^2$ must exceed some positive constant C_G , that is, $\text{Tr}[\mathbf{H} \mathbf{W}_{\text{whitened}}^{(t)}]^2 > C_G$.

On the other hand, because:

1. The quadratic loss term $\text{Tr}[(\mathbf{W}_{\text{whitened}}^{(t)})^\top \mathbf{H} \mathbf{W}_{\text{whitened}}^{(t)}]$ is upper-bounded on $\mathbb{R}^{n \times n}$, and
2. $\text{Tr}[(\mathbf{W}_{\text{whitened}}^{(t)})^\top \mathbf{H} \mathbf{W}_{\text{whitened}}^{(t)}] \neq 0$ (due to $\mathbf{W}_{\text{whitened}}^{(t)} \neq \mathbf{W}^*$),

we have that there exists a positive number $0 < C_{\mathcal{L}}$ such that

$$0 < \text{Tr}[(\mathbf{W}_{\text{whitened}}^{(t)})^\top \mathbf{H} \mathbf{W}_{\text{whitened}}^{(t)}] < C_{\mathcal{L}}.$$

Finally, since the norm of \mathbf{H} is upper bounded, its trace must also be upper bounded by some constant C_H . Therefore, putting everything together, we have:

$$Q > \frac{C_G^2}{C_{\mathcal{L}} C_H}.$$

This inequality holds even as the condition number $\kappa \rightarrow +\infty$. \square

F PROOF OF PROPOSITION 3

To prove Proposition 3, we first generalize existing work on the convergence rate lower bound (via contraction factor) of gradient descent and Adam (we only consider $\beta_2 = 1$) under the same setting:

Theorem 4 (Contraction factor lower bound for gradient descent, generalized based on Zhang et al. (2024)). *Consider the optimization problem in Equation (12). Let \mathbf{W}_{GD}^t be the output of GD after t steps. Then, for any step size η , there exists an initial condition such that the following lower bound on the contraction rate holds:*

$$\mathcal{L}(\mathbf{W}_{GD}^{t+1}) - \mathcal{L}^* \geq \left(1 - \frac{2}{\kappa + 1}\right) (\mathcal{L}(\mathbf{W}_{GD}^t) - \mathcal{L}^*),$$

where $\mathcal{L}^* = \mathcal{L}(\mathbf{W}^*)$. Furthermore, under optimal $\eta = \frac{2}{\lambda_1 + \lambda_m}$, the bound becomes tight regardless of the settings of \mathbf{H} , where λ_1 and λ_m are the largest and smallest eigen values of \mathbf{H} , respectively.

Proof. The proposition 1 in Zhang et al. (2024) has shown that the lower bound holds for diagonal positive definite Hessian \mathbf{H} . To show that the lower bound holds for a general positive definite Hessian \mathbf{H} we will reformulate the problem to align with the setup in diagonal case (Proposition 1 of Zhang et al. (2024)).

First, for any positive definite Hessian \mathbf{H} , we can perform an eigen decomposition $\mathbf{H} = \mathbf{U}\mathbf{S}\mathbf{U}^\top$, where \mathbf{U} is an orthogonal matrix and \mathbf{S} is a diagonal matrix containing the eigenvalues of \mathbf{H} . Define a change of variables $\mathbf{Z} = \mathbf{U}^\top \mathbf{W}$. Then, the optimization problem becomes

$$\mathcal{L}(\mathbf{Z}) = \frac{1}{2} \text{Tr}(\mathbf{Z}^\top \mathbf{S} \mathbf{Z}),$$

which reduces the problem to the case of a diagonal \mathbf{H} with condition number $\kappa = \frac{\lambda_1}{\lambda_m}$, where λ_1 and λ_m are the largest and smallest eigenvalues of \mathbf{H} , respectively.

Thus, by applying Proposition 1 of Zhang et al. (2024) to this transformed problem, we conclude that there exists initial point such that the lower bound on the contraction rate

$$\mathcal{L}(\mathbf{W}_{GD}^{(t+1)}) - \mathcal{L}^* \geq \left(1 - \frac{2}{\kappa + 1}\right) (\mathcal{L}(\mathbf{W}_{GD}^{(t)}) - \mathcal{L}^*)$$

holds for the transformed variables \mathbf{Z} and, equivalently, for the original variables \mathbf{W} since the condition number is preserved under orthogonal transformations.

Therefore, the lower bound for gradient descent applies to any general positive definite Hessian \mathbf{H} provided the condition number κ remains unchanged.

Finally, under the optimal step size $\eta = \frac{2}{\lambda_1 + \lambda_m}$, the bound becomes tight regardless of the settings of \mathbf{H} . This is achieved by selecting η to minimize the contraction factor, aligning with well-known results regarding the optimal convergence rate of gradient descent on quadratic objectives (Nesterov, 2013).

This completes the proof of Theorem 4. \square

Corollary 1 (Lower bound on Adam ($\beta_2 = 1$)). *Consider the optimization problem in Equation (12). Assume the weight initialization \mathbf{W}^0 assigned zero probability to any set of zero Lebesgue measure in $\mathbb{R}^{m \times n}$. Let $\mathbf{W}_{Adam}^{(t)}$ be the parameter after t iterations of Adam with hyperparameters $\beta_1 = 0$ and $\beta_2 = 1$. Then, for any step size η , the following lower bound on the contraction rate holds:*

$$\mathcal{L}(\mathbf{W}_{Adam}^{(t+1)}) - \mathcal{L}^* \geq \left(1 - \frac{2}{\kappa'(\mathbf{W}^0) + 1}\right) (\mathcal{L}(\mathbf{W}_{Adam}^{(t)}) - \mathcal{L}^*),$$

where $\kappa'(\mathbf{W}^0)$ is the \mathbf{W}^0 -dependent condition number of the preconditioned Hessian $\text{diag}(|\mathbf{H}\mathbf{W}^0|^{-1})\mathbf{H}$, and $\mathcal{L}^* = \mathcal{L}(\mathbf{W}^*)$.

Proof. The update rule of Adam with $\beta_1 = 0$ and $\beta_2 = 1$ is given by Zhang et al. (2024):

$$\mathbf{W}_{Adam}^{(t+1)} = \mathbf{W}_{Adam}^{(t)} + \eta \text{diag}(|\mathbf{H}\mathbf{W}^{(0)}|^{-1}) \mathbf{H} \mathbf{W}_{Adam}^{(t)}.$$

This can be interpreted as gradient descent with a preconditioned Hessian matrix $\text{diag}(|\mathbf{H}\mathbf{W}^{(0)}|^{-1})\mathbf{H}$. By applying Theorem 4, we conclude that the contraction rate for Adam under these settings satisfies the lower bound:

$$\mathcal{L}(\mathbf{W}_{\text{Adam}}^{(t+1)}) - \mathcal{L}^* \geq \left(1 - \frac{2}{\kappa + 1}\right) \left(\mathcal{L}(\mathbf{W}_{\text{Adam}}^{(t)}) - \mathcal{L}^*\right),$$

where κ is the condition number of the Hessian matrix \mathbf{H} .

Therefore, the proof is complete. \square

Next, We extend our Theorem 3 to block-diagonal Hessian case to prepare for discussions on group learning rates when comparing to Adam.

Corollary 2 (Upper Bound Convergence Rate of SWAN). *Consider the same quadratic loss function $\mathcal{L}(\mathbf{W}) = \frac{1}{2}\text{Tr}(\mathbf{W}^\top \mathbf{H}\mathbf{W})$ with \mathbf{H} being block-diagonal. That is, $\mathbf{H} = \text{diag}(\mathbf{H}_1, \mathbf{H}_2, \dots, \mathbf{H}_L)$, where each $\mathbf{H}_l \in \mathbb{R}^{m_l \times n_l}$ is a positive definite matrix for $l = 1, 2, \dots, L$, and $\sum_{l=1}^L m_l = m$ and $\sum_{l=1}^L n_l = n$. Assume the initialization distribution of $\mathbf{W}^{(0)}$ assigns zero probability to any zero measure set in $\mathbb{R}^{m \times n}$. Let $\mathbf{W}_{\text{whitened}}^{(t)}$ be the parameter matrix after t iterations of the SWANoptimizer defined in Theorem 3, with learning rate η . Then, under the conditions that ⁶:*

$$\|\mathbf{H}_l \mathbf{W}_l^{(t)}\|_1^2 - \text{Tr}(\mathbf{H}_l) \cdot \text{Tr}((\mathbf{W}_l^{(t)})^\top \mathbf{H}_l \mathbf{W}_l^{(t)}) \cdot \frac{2\lambda_{l,m_l}}{\lambda_{l,1} + \lambda_{l,m_l}} > 0,$$

where $\lambda_{l,1}$ and λ_{l,m_l} are the largest and smallest singular value of \mathbf{H}_l , respectively; then there exists a proper learning rate η such that: with probability 1, the loss satisfies:

$$\mathcal{L}(\mathbf{W}_{\text{whitened}}^{(t+1)}) - \mathcal{L}^* < \max_{l \in [L]} \left(1 - \frac{2}{\kappa_l + 1}\right) \left(\mathcal{L}(\mathbf{W}_{\text{whitened}}^{(t)}) - \mathcal{L}^*\right), \quad (21)$$

where κ_l is the condition number of \mathbf{H}_l .

Proof. Applying the arguments in the proof of Theorem 3 to each block l , we have (for simplicity, we will drop the subscript “whitened” when there is no confusion):

$$\begin{aligned} \frac{\mathcal{L}(\mathbf{W}_l^{(t+1)}) - \mathcal{L}^*}{\mathcal{L}(\mathbf{W}_l^{(t)}) - \mathcal{L}^*} &= 1 - \frac{\mathcal{L}(\mathbf{W}_l^{(t)}) - \mathcal{L}(\mathbf{W}_l^{(t+1)})}{\mathcal{L}(\mathbf{W}_l^{(t)}) - \mathcal{L}^*} \\ &= 1 - \frac{\eta \|\mathbf{H}_l \mathbf{W}_l^{(t)}\|_1 - \frac{\eta^2}{2} \text{Tr}(\mathbf{H}_l)}{\frac{1}{2} \text{Tr}[(\mathbf{W}_l^{(t)})^\top \mathbf{H}_l \mathbf{W}_l^{(t)})]}. \end{aligned}$$

It is straightforward to verify via the quadratic formula that if one chooses η satisfying:

$$\begin{aligned} &\frac{\|\mathbf{H}_l \mathbf{W}_l^{(t)}\|_1 - \sqrt{\|\mathbf{H}_l \mathbf{W}_l^{(t)}\|_1^2 - \text{Tr}(\mathbf{H}_l) \cdot \text{Tr}((\mathbf{W}_l^{(t)})^\top \mathbf{H}_l \mathbf{W}_l^{(t)}) \cdot \frac{2\lambda_{l,m_l}}{\lambda_{l,1} + \lambda_{l,m_l}}}}{\text{Tr}(\mathbf{H}_l)} < \eta \\ &< \frac{\|\mathbf{H}_l \mathbf{W}_l^{(t)}\|_1 + \sqrt{\|\mathbf{H}_l \mathbf{W}_l^{(t)}\|_1^2 - \text{Tr}(\mathbf{H}_l) \cdot \text{Tr}((\mathbf{W}_l^{(t)})^\top \mathbf{H}_l \mathbf{W}_l^{(t)}) \cdot \frac{2\lambda_{l,m_l}}{\lambda_{l,1} + \lambda_{l,m_l}}}}{\text{Tr}(\mathbf{H}_l)}, \end{aligned}$$

then we have:

$$\frac{\frac{1}{2} \text{Tr}[(\mathbf{W}_l^{(t)})^\top \mathbf{H}_l \mathbf{W}_l^{(t)})]}{\eta \|\mathbf{H}_l \mathbf{W}_l^{(t)}\|_1 - \frac{\eta^2}{2} \text{Tr}(\mathbf{H}_l)} < \frac{\kappa_l + 1}{2}.$$

⁶Note that according to Proposition 2, this is always achievable when \mathbf{H}_l is poorly-conditioned ($\frac{\lambda_{l,d_l}}{\lambda_{l,1}}$ is small enough). The lower interval above converges to zero, and one can simply pick e.g., $\eta = \min_{l \in [L]} \frac{\text{Tr}(\mathbf{H}_l \mathbf{W}_l^{(t)})}{\text{Tr}(\mathbf{H}_l)}$.

Rearranging, we obtain:

$$\frac{\mathcal{L}(\mathbf{W}_l^{(t+1)}) - \mathcal{L}^*}{\mathcal{L}(\mathbf{W}_l^{(t)}) - \mathcal{L}^*} < 1 - \frac{2}{\kappa_l + 1}.$$

Since \mathbf{H} is block-diagonal, the updates for each block l are independent. Summing the loss over all blocks, we obtain:

$$\mathcal{L}(\mathbf{W}_{\text{whitened}}^{(t+1)}) - \mathcal{L}^* = \sum_{l=1}^L \left(\mathcal{L}(\mathbf{W}_l^{(t+1)}) - \mathcal{L}^* \right) < \sum_{l=1}^L \left(1 - \frac{2}{\kappa_l + 1} \right) \left(\mathcal{L}(\mathbf{W}_l^{(t)}) - \mathcal{L}^* \right).$$

Taking the maximum contraction factor across all blocks:

$$\begin{aligned} \mathcal{L}(\mathbf{W}_{\text{whitened}}^{(t+1)}) - \mathcal{L}^* &< \max_{l \in [L]} \left(1 - \frac{2}{\kappa_l + 1} \right) \sum_{l=1}^L \left(\mathcal{L}(\mathbf{W}_l^{(t)}) - \mathcal{L}^* \right) \\ &= \max_{l \in [L]} \left(1 - \frac{2}{\kappa_l + 1} \right) \left(\mathcal{L}(\mathbf{W}_{\text{whitened}}^{(t)}) - \mathcal{L}^* \right). \end{aligned}$$

Thus, the overall contraction factor for the SWANoptimizer is:

$$\rho_{\text{SWAN}} = \max_{l \in [L]} \left(1 - \frac{2}{\kappa_l + 1} \right).$$

□

Finally, we are ready to prove Proposition 3:

Proposition 2 (GradWhitening with single lr vs Adam with tuned group lr). *Consider the optimization problem Equation (12). Assume \mathbf{H} is block-diagonal, i.e., $\mathbf{H} = \text{diag}(\mathbf{H}_1, \mathbf{H}_2, \dots, \mathbf{H}_L)$, where each $\mathbf{H}_l \in \mathbb{R}^{m_l \times m_l}$ is a positive definite matrix for $l = 1, 2, \dots, L$, and $\sum_{l=1}^L m_l = m$. Assuming for GradWhitening we use one global learning rate for all parameters; and for Adam, we use the optimally chosen group learning rate η_l and initial condition w_0 for each block \mathbf{H}_l . Assume either if i) certain regularity conditions are met (see proof in Appendix), or ii), if \mathbf{H} is poorly-conditioned (its condition number is large enough). Then: regardless of its initialization, GradWhitening with a properly chosen learning rate will still have a strictly better convergence speed (i.e., smaller contraction factor) across all blocks $l \in [L]$ than Adam ($\beta_1 = 0, \beta_2 = 1$) under optimal group-wise learning rates and initial condition.*

Proof. For simplicity, we will drop the subscript “whitened” when there is no confusion. Let $\kappa'_l(\mathbf{W}_l^{(0)})$ denote the $\mathbf{W}_l^{(0)}$ -dependent condition number of the l -th block preconditioned Hessian $\text{diag}(\left| \mathbf{H}_l \mathbf{W}_l^{(0)} \right|^{-1} \mathbf{H}_l)$. Let $\lambda_{l,m_l}(\mathbf{W}_l^{(0)})$ and $\lambda_{l,1}(\mathbf{W}_l^{(0)})$ be the smallest and largest eigenvalues of $\text{diag}(\left| \mathbf{H}_l \mathbf{W}_l^{(0)} \right|^{-1} \mathbf{H}_l)$, respectively. Then,

Case 1: Under the conditions that:

1. **Existence of roots:** $\forall l \in [L]$,

$$\|\mathbf{H}_l \mathbf{W}_l^{(t)}\|_1^2 - \text{Tr}(\mathbf{H}_l) \cdot \text{Tr} \left((\mathbf{W}_l^{(t)})^\top \mathbf{H}_l \mathbf{W}_l^{(t)} \right) \cdot \frac{2\lambda_{l,m_l}(\mathbf{W}_l^{(0)})}{\lambda_{l,1}(\mathbf{W}_l^{(0)}) + \lambda_{l,m_l}(\mathbf{W}_l^{(0)})} > 0,$$

and

2. **Overlap condition:**

$$\begin{aligned} &\min_{l \in [L]} \frac{\text{Tr}(\mathbf{H}_l \mathbf{W}_l^{(t)}) + \sqrt{\text{Tr}(\mathbf{H}_l \mathbf{W}_l^{(t)})^2 - \text{Tr}(\mathbf{H}_l) \cdot \text{Tr} \left((\mathbf{W}_l^{(t)})^\top \mathbf{H}_l \mathbf{W}_l^{(t)} \right) \cdot \frac{2\lambda_{l,m_l}(\mathbf{W}_l^{(0)})}{\lambda_{l,1}(\mathbf{W}_l^{(0)}) + \lambda_{l,m_l}(\mathbf{W}_l^{(0)})}}{\text{Tr}(\mathbf{H}_l)} \\ &> \max_{l \in [L]} \frac{\text{Tr}(\mathbf{H}_l \mathbf{W}_l^{(t)}) - \sqrt{\text{Tr}(\mathbf{H}_l \mathbf{W}_l^{(t)})^2 - \text{Tr}(\mathbf{H}_l) \cdot \text{Tr} \left((\mathbf{W}_l^{(t)})^\top \mathbf{H}_l \mathbf{W}_l^{(t)} \right) \cdot \frac{2\lambda_{l,m_l}(\mathbf{W}_l^{(0)})}{\lambda_{l,1}(\mathbf{H}_l^{(0)}) + \lambda_{l,m_l}(\mathbf{W}_l^{(0)})}}{\text{Tr}(\mathbf{H}_l)}. \end{aligned}$$

Then, there exists a global learning rate η , such that for all $l \in [L]$,

$$\frac{\mathcal{L}(\mathbf{W}_{\text{whitened}}^{(t+1)})_l - \mathcal{L}_l^*}{\mathcal{L}(\mathbf{W}_{\text{whitened}}^{(t)})_l - \mathcal{L}_l^*} < 1 - \frac{2}{\kappa'_l(\mathbf{W}_l^{(0)}) + 1} \leq \frac{\mathcal{L}(\mathbf{W}_{\text{Adam}}^{(t+1)})_l - \mathcal{L}_l^*}{\mathcal{L}(\mathbf{W}_{\text{Adam}}^{(t)})_l - \mathcal{L}_l^*}.$$

Case 2: If \mathbf{H} is poorly-conditioned, i.e., $\frac{\lambda_{l,m_l}(\mathbf{W}_l^{(0)})}{\lambda_{l,1}(\mathbf{W}_l^{(0)})} \rightarrow 0$, then Proposition 2 asserts that the following term

$$\max_{l \in [L]} \frac{\text{Tr}(\mathbf{H}_l \mathbf{W}_l^{(t)}) - \sqrt{\text{Tr}(\mathbf{H}_l \mathbf{W}_l^{(t)})^2 - \text{Tr}(\mathbf{H}_l) \cdot \text{Tr}((\mathbf{W}_l^{(t)})^\top \mathbf{H}_l \mathbf{W}_l^{(t)})} \cdot \frac{2\lambda_{l,m_l}(\mathbf{W}_l^{(0)})}{\lambda_{l,1}(\mathbf{W}_l^{(0)}) + \lambda_{l,m_l}(\mathbf{W}_l^{(0)})}}{\text{Tr}(\mathbf{H}_l)} \rightarrow 0,$$

and one can simply choose, for example, $\eta = \min_{l \in [L]} \frac{\text{Tr}(\mathbf{H}_l \mathbf{W}_l^{(t)})}{\text{Tr}(\mathbf{H}_l)}$. Under this choice of η , we still have

$$\frac{\mathcal{L}(\mathbf{W}_{\text{whitened}}^{(t+1)})_l - \mathcal{L}_l^*}{\mathcal{L}(\mathbf{W}_{\text{whitened}}^{(t)})_l - \mathcal{L}_l^*} < 1 - \frac{2}{\kappa'_l(\mathbf{W}_l^{(0)}) + 1} \leq \frac{\mathcal{L}(\mathbf{W}_{\text{Adam}}^{(t+1)})_l - \mathcal{L}_l^*}{\mathcal{L}(\mathbf{W}_{\text{Adam}}^{(t)})_l - \mathcal{L}_l^*}$$

for all $l \in [L]$. \square

G PROOF OF PROPOSITION 1

Proof. First, define $\mathbf{V} \in \mathbb{R}^{M_C \times n}$ as $\mathbf{V} := \mathbf{U}_C^\top \mathbf{W}$, and consider the Hessian with respect to \mathbf{V} instead of \mathbf{W} . Notice that although the loss function \mathcal{L} is unknown, its first-order derivatives are known. Specifically, they are given by:

$$\frac{\partial \mathcal{L}}{\partial v_{lk}} = \dot{v}_{lk} = \mathbb{E}_{q=m} [g_{h_k} x_l] e^{\frac{1}{2} \sum_s v_{ls}^2}.$$

Therefore, the second-order derivatives, i.e., the Hessian matrix $\mathbf{H}(\mathbf{V})$, are:

$$\mathbf{H}(\mathbf{V})_{lk, l'k'} = \frac{\partial^2 \mathcal{L}}{\partial v_{lk} \partial v_{l'k'}} = \frac{\partial \left[\mathbb{E}_{q=m} [g_{h_k} x_l] e^{\frac{1}{2} \sum_s v_{ls}^2} \right]}{\partial v_{l'k'}} = \dot{v}_{lk} v_{l'k'} \delta_{ll'},$$

where $\delta_{ll'}$ is the Kronecker delta, which is 1 if $l = l'$ and 0 otherwise.

Based on Lemma B.6 in Zhao et al. (2024a), as $t \rightarrow \infty$, there exists an index subset $O_l \subset \{1, \dots, M_C\}$ such that:

$$v_{l^*k} \gg v_{lk}, \quad \dot{v}_{l^*k} \gg \dot{v}_{lk}, \quad \forall l^* \in O_l, l \notin O_l, \forall k.$$

Consequently,

$$\mathbf{H}(\mathbf{V})_{l^*k, l^*k'} \gg \mathbf{H}(\mathbf{V})_{lk, l'k'}, \quad \forall l^* = l'^* \in O_l, l, l' \notin O_l, \forall k, k'.$$

After normalization, as $t \rightarrow \infty$, we have

$$\frac{\mathbf{H}(\mathbf{V})_{lk, l'k'}}{\sum_{l, l'} \mathbf{H}(\mathbf{V})_{lk, l'k'}} \xrightarrow{t \rightarrow \infty} \begin{cases} 1, & \text{if } l = l' \in O_l, \\ 0, & \text{otherwise.} \end{cases}$$

Reverting back to the \mathbf{W} space, we have

$$\mathbf{H}(\mathbf{W}) = (\mathbf{I}_K \otimes \mathbf{U}_C) \mathbf{H}(\mathbf{V}) (\mathbf{I}_K \otimes \mathbf{U}_C)^\top,$$

where \otimes denotes the Kronecker product and \mathbf{I}_K is the identity matrix of appropriate dimensions.

Therefore, for all $1 \leq s, s' \leq d$ and $1 \leq k, k' \leq n$, we obtain

$$\frac{\mathbf{H}(\mathbf{W})_{sk, s'k'}}{\sum_{s, s'} \mathbf{H}(\mathbf{W})_{sk, s'k'}} = \frac{\mathbf{H}(\mathbf{W})_{sk', s'k'}}{\sum_{s, s'} \mathbf{H}(\mathbf{W})_{sk', s'k'}} \quad \text{as } t \rightarrow \infty.$$

This holds for all $1 \leq s, s' \leq d$ and $1 \leq k, k' \leq n$. \square

H PROOF OF THEOREM 2

Proof. Assume that we have a function $f(\mathbf{W})$ defined on $\mathbf{W} \in \mathbb{R}^{m \times n}$ that we want to minimize, and the global minimum is at \mathbf{W}^* (without loss of generality, let $\mathbf{W}^* = 0$). Then our problem can be written as:

$$\min_{\mathbf{W} \in \mathbb{R}^{m \times n}} f(\mathbf{W}) \quad (22)$$

Assume f is a twice differentiable function and has a Lipschitz continuous Hessian around \mathbf{W}^* , then both GradWhitening and Newton's method approximate the loss equation 22 up to second order (ignoring first-order terms without loss of generality) as:

$$\min_{\mathbf{w} \in \mathbb{R}^{mn}} \frac{1}{2} \mathbf{w}^T \mathbf{H} \mathbf{w}, \quad (23)$$

where $\mathbf{w} \in \mathbb{R}^{mn \times 1}$ is the flattened version of \mathbf{W} , and $\mathbf{H} \in \mathbb{R}^{mn \times mn}$ is the Hessian matrix of f at \mathbf{W}^* . We may apply second-order Newton's method to optimize equation 23, which gives the following update:

$$\mathbf{w}^{t+1} = \mathbf{w}^t - \eta \mathbf{H}^{-1} \nabla f(\mathbf{w}^t). \quad (24)$$

However, this update is very expensive and requires $\mathcal{O}(m^3 n^3)$ computation. SWAN can then be viewed as a fast approximation to estimate the update of equation 24. Under our assumption on Hessian structure, we have:

$$\mathbf{H} = \text{diag}(\tilde{\mathbf{H}}, \tilde{\mathbf{H}}, \dots, \tilde{\mathbf{H}}, \dots, \tilde{\mathbf{H}}) \quad (25)$$

where $\tilde{\mathbf{H}} \in \mathbb{R}^{m \times m}$.

Under this assumption, the optimization problem equation 23 can be rewritten as:

$$\min_{\mathbf{W} \in \mathbb{R}^{m \times n}} \frac{1}{2} \text{Tr} \left[\mathbf{W}^T \tilde{\mathbf{H}} \mathbf{W} \right], \quad (26)$$

For this model, the gradient of \mathbf{W} is given by:

$$\nabla f(\mathbf{W}) = \tilde{\mathbf{H}} \mathbf{W}.$$

Let \mathbf{W} have rank m , and assume $n > m$. We say \mathbf{W} is now *over-parameterized* in the sense that its dimensionality is now larger than the dimensionality of the second-order information $\tilde{\mathbf{H}}$. It is now clear that the second-order information is *losslessly compressed* into gradients: one can exactly recover the Hessian via

$$\mathbf{H} = \text{diag}(\nabla f(\mathbf{W}) \mathbf{W}^{-1}, \nabla f(\mathbf{W}) \mathbf{W}^{-1}, \dots, \nabla f(\mathbf{W}) \mathbf{W}^{-1}, \dots, \nabla f(\mathbf{W}) \mathbf{W}^{-1}).$$

Given this fact, one can easily estimate Newton's update $\mathbf{H}^{-1} \nabla f(\mathbf{w}^t)$ without explicitly estimating \mathbf{H}^{-1} (or $\tilde{\mathbf{H}}$). Notice that:

$$\mathbf{H} = \mathbf{I}_m \otimes \tilde{\mathbf{H}}$$

where \mathbf{I}_m is the $m \times m$ identity matrix and \otimes denotes the Kronecker product. Given that

$$\mathbf{H}^{-1} = \mathbf{I}_m \otimes \tilde{\mathbf{H}}^{-1},$$

we have

$$\mathbf{H}^{-1} \nabla f(\mathbf{w}^t) = (\mathbf{I}_m \otimes \tilde{\mathbf{H}}^{-1}) \text{vec}(\nabla f(\mathbf{W}^t)) = \text{vec} \left(\tilde{\mathbf{H}}^{-1} \nabla f(\mathbf{W}^t) \right).$$

Reshaping back to matrix form, we can rewrite the update rule as:

$$\tilde{\mathbf{H}}^{-1} \nabla f(\mathbf{W}^t).$$

Next, since $\tilde{\mathbf{H}}$ is positive definite:

$$\nabla f(\mathbf{W}^t) = \tilde{\mathbf{H}}\mathbf{W}^t = \mathbf{Q}\Lambda\mathbf{Q}^\top\mathbf{W}^t,$$

where $\mathbf{Q}\Lambda\mathbf{Q}^\top$ is the eigen decomposition of $\tilde{\mathbf{H}}$. Assume further that \mathbf{W}^t is initialized as orthogonal; one can immediately recognize that \mathbf{Q} is also the left singular vector matrix of $\nabla f(\mathbf{W}^t)$. Therefore, the matrix inversion of $\tilde{\mathbf{H}}$ required in Newton’s update equation 24 can be easily achieved by simply deleting the Λ term. That is,

$$\begin{aligned} \tilde{\mathbf{H}}^{-1}\nabla f(\mathbf{W}^t) &= \mathbf{Q}\Lambda^{-1}\mathbf{Q}^\top\mathbf{Q}\Lambda\mathbf{Q}^\top\mathbf{W}^t \\ &= \mathbf{Q}[\mathbf{Q}^\top\mathbf{W}^t] \stackrel{\mathbf{U}:=\mathbf{Q}, \mathbf{V}:=\mathbf{W}^t}{=} \mathbf{Q}\mathbf{U}\mathbf{V}^\top = \mathcal{P}(\nabla f(\mathbf{W}^t)) = \mathbf{G}_{\text{whitened}}. \end{aligned}$$

This is exactly the GradWhitening-modified gradient update. \square

I IMPLEMENTATION DETAILS

Setup We describe the implementation setups for SWAN used in LLM pre-training tasks. To enable a more straightforward and comparable analysis, we simply replicate the setting of Zhao et al. (2024a), under exactly the same model configs and optimizer configs. This include the same model architecture, tokenizer, batch size, context length, learning rate scheduler, etc. The only exception is that since SWAN does not need warm up, we use zero-warm up ratio for SWAN. But we still ensure that the learning rates of all methods are fully decayed to the same target learning rate ($0.1 \times$ initial learning rate). Across all model sizes, we use the same hyperparameter settings and the same learning rate tuning procedure. The only exception is that for model of size 1.3B: as we already know that larger model requires smaller learning rates, we conduct learning search for Adam and Galore over a smaller but more fine grained grid of $\{0.001, 0.0007, 0.0005, 0.0003, 0.0001\}$. As a result, the optimal learning rate found for Adam on 1.3B is 0.0007.

Applying SWAN on LLMs Since SWAN utilizes matrix-level operations on gradients, it can only be applied on 2D parameters. Therefore, in our experiments we only apply *SWAN* on all linear projection weights in transformer blocks. Similar to Galore (Zhao et al., 2024a), the rest of the non-Linear parameters still uses Adam as default choice. Therefore, we follow the learning rate setup of Galore, where we fix a global learning rate 0.001 across all model sizes and all modules. Then, for the linear projection modules where SWAN is applied, we simply apply a scaling factor α on top of the global learning rate. We choose $\alpha = 1$ for all model sizes except for 1.3 B case, where we used $\alpha = 0.3$, resulting an effective learning rate of 0.0003. Note that this choice is quite random; and it is not extensively grid-searched.

Applying GradWhitening We found that one strategy that lead to better convergence is to first convert the gradient matrix to FP32, perform GradWhitening, and then convert back to BF16. This is the default setup in Section 5. In practice, we found that using a step size $\beta \neq 0.5$ in the GradWhitening operator (Algorithm 2) can improve its convergence. We found that setting $\beta = 0.8$ with iteration number $k = 10$ generally give satisfactory performance. This can be further optimized and we leave it for future work. Alternatively, GradWhitening can also be done in BF16 precision. The setup we use for BF16 precision is $\beta = 0.85$, $k = 6$. These hyperparameters are selected on randomly sampled matrices via minimizing inverse square root estimation loss; then directly applied to LLM without any further tuning. We found that this usually translates well.